

AD-A124 790

PLASMA ELECTRON NUMBER DENSITY AND ELECTRON-NEUTRAL
COLLISION FREQUENCY F..(U) AIR FORCE INST OF TECH
WRIGHT-PATTERSON AFB OH SCHOOL OF ENGI.. T W HERMANSON
DEC 82 AFIT/GEP/PH/82D-12

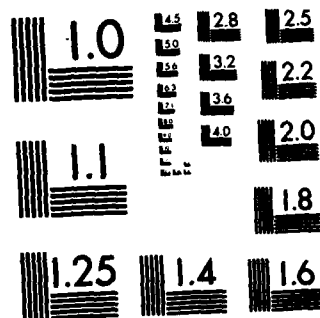
1/1

UNCLASSIFIED

F/G 20/9

NL

END
DATE
FILMED
83
DTIC



MICROCOPY RESOLUTION TEST CHART
NATIONAL BUREAU OF STANDARDS-1963-A

AD A124690



DEPARTMENT OF THE AIR FORCE
AIR UNIVERSITY (ATC)

AIR FORCE INSTITUTE OF TECHNOLOGY

Wright-Patterson Air Force Base, Ohio

THIS DOCUMENT HAS BEEN REPRODUCED
EXACTLY AS RECEIVED AND WITH NO
EDITING OR REVISIONS.

83 03 020123

DTIC
ELECTE
FEB 23 1964

S D

E

FILE COPY

①

PLASMA ELECTRON NUMBER DENSITY AND
ELECTRON-NEUTRAL COLLISION FREQUENCY
FROM COMPLEX IMPEDANCE MEASUREMENTS

THESIS

AFIT/GEP/PH/82D-12 THOMAS W. HERMANSON
CAPTAIN USAF

DTIC
SELECTE
S E

Approved for public release; distribution unlimited

AFIT/GEP/PH/82D-12

PLASMA ELECTRON NUMBER DENSITY AND
ELECTRON-NEUTRAL COLLISION FREQUENCY
FROM COMPLEX IMPEDANCE MEASUREMENTS

THESIS

Presented to the Faculty of the School of Engineering
of the Air Force Institute of Technology
Air University
in Partial Fulfillment of the
Requirements for the Degree of
Master of Science

by

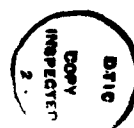
THOMAS W. HERMANSON

CAPTAIN USAF

Graduate Engineering Physics

December 1982

Approved for public release; distribution unlimited



Accession For	
NTIS GRA&I	<input checked="checked" type="checkbox"/>
DTIC TAB	<input type="checkbox"/>
Unannounced	<input type="checkbox"/>
Justification	
By	
Distribution/	
Availability Codes	
Dist	Avail and/or Special
A	

Preface

The objective of this thesis was to determine plasma electron number density and electron-neutral collision frequency from the measurement of the complex impedance of a radio frequency (RF) plasma discharge within a barrel type reactor under specified operating conditions (gas type, pressure, RF power level).

This report is limited to a specific plasma model and impedance measurement technique. The choice of model and experimental configuration was found to limit the accuracy of impedance measurements when applied to order-of-magnitude ranges of frequency or power. Application to the general class of inductively driven plasma reactors shows the most promise of success when the specific reactor can be isolated from stray capacitive effects.

I would like to express appreciation to Dr. Peter Bletzinger and the Air Force Wright Aeronautical Labs for suggesting and sponsoring this study and to Lt Col William F. Bailey, for his professional insight and assistance. I would also like to thank Ms. Barbara A. Graham and my brother, William F. Hermanson, for their graphical, clerical, and moral support.

(This document was typed by Ms. Barbara A. Graham)

Table of Contents

	<u>Page</u>
Preface.....	ii
List of Figures.....	iv
List of Symbols.....	vi
Abstract.....	vii
I. Introduction.....	1
Background.....	1
Problem Statement.....	6
Scope and Assumptions.....	6
General Approach and Organization.....	8
II. Theory.....	10
III. Equipment.....	31
Plasma Tube.....	31
Vacuum System.....	32
Electrical System.....	34
Optical Diagnostic System.....	34
Configuration.....	36
IV. Procedure.....	38
V. Results.....	41
Plasma-Circuit Interaction.....	41
Model Validation.....	41
Application.....	42
VI. Conclusion.....	56
Summary and Conclusions.....	56
Recommendations.....	61
Bibliography.....	64
Appendix A: Data Reduction.....	65
Appendix B: Data Reduction.....	67
Appendix C: Computer Programs.....	72
Vita.....	77

List of Figures

<u>Figures</u>		<u>Page</u>
1.	Plasma Reactors.....	2
2.	RF Reactors.....	4
3.	Equipment Layout.....	9
4.	Plasma Model.....	23
5.	Plasma Tube.....	31
6.	Vacuum System.....	33
7.	Electrical System.....	35
8.	Optical System.....	37
9.	Equipment Layout.....	37
10.	Impedance Measurement.....	39
11.	Real Impedance Component.....	43
12.	Imaginary Impedance Component.....	44
13.	Real Impedance Component.....	45
14.	Imaginary Impedance Component.....	46
15.	Real Admittance Component.....	48
16.	Imaginary Admittance Component.....	49
17.	Collision Frequency.....	51
18.	Number Density.....	52
19.	Collision Frequency.....	53
20.	Number Density.....	54
21.	Line Intensities.....	55
22.	Modified Model.....	61
23.	Compacitive Reactor Design.....	63
24.	Capacitor Calibration.....	69

Figures

Page

25.	Capacitor Calibration.....	70
26.	Inductor Calibration.....	71

List of Symbols

C_o	Capacitive component interior to the plasma tube
C_B	Capacitive component exterior to the plasma tube
L	Inductance
ϵ_p	Relative permittivity of the plasma
Z	Impedance
R_p	Real part of a complex impedance
X_p	Imaginary part of a complex impedance
Z_e	Equivalent impedance of a circuit
Z_p	Impedance of the plasma model
ω	Angular frequency
ω_p	Plasma frequency
ν	Electron-neutral collision frequency
n	Electron number density
σ	Cross section
p	Pressure
γ	Numerical constant
α	Numerical constant

Abstract

↓
The plasma within an RF driven inductive coil interacts with the electrical generation circuit providing feedback useful for control of bulk plasma parameters. An investigation, employing a tunable RF circuit, was made applying complex impedance measurements as a plasma diagnostic. Plasma-circuit effects are modeled as capacitive coupling to the driving inductor; the magnitude of the plasma model capacitance being proportional to a complex plasma permittivity. Associated impedance, when annulled by tuning, results in a real resistive load dependent upon plasma characteristics. Impedance diagnostics avoid the use of traditional internal probes. Application of this technique to inductive reactors is found to be inferior to capacitive reactors.
↑

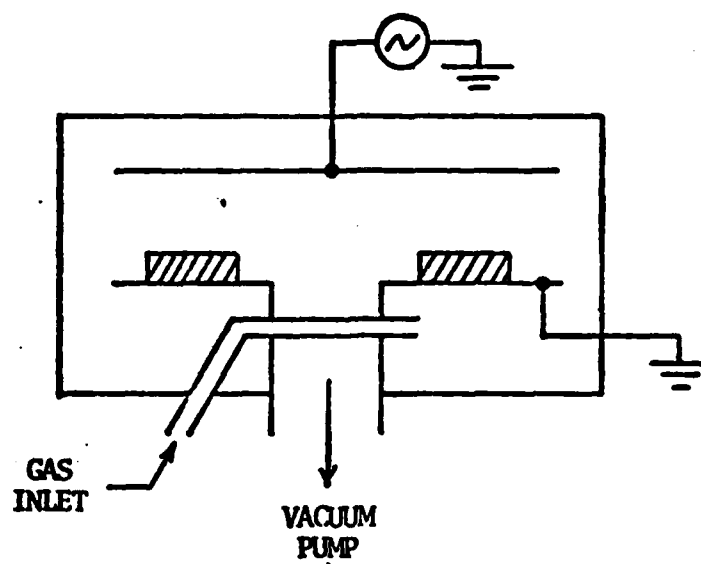
I. Introduction

Background

Plasma reactors are used extensively in the manufacture of integrated circuits and thin film solar collectors. Within the reactor a plasma is formed when energy is transferred to a low pressure gas through the application of a radio frequency (RF) electric field. Subsequent molecular dissociation, ionization and particle redistribution make possible the etching or deposition of desired substances onto receiver substrates used for integrated circuit production.

Plasma reactors applicable to RF processes are distinguished by physical geometry and method of excitation. Two reactor configurations which are used in industry are the parallel plate type and the barrel type. The latter lends itself to application in large scale production processes. Figure 1 is a schematic of two reactor types used by the Hewlett-Packard Corporation. Reactant gas is bled into a chamber being evacuated by pumps. An RF varying potential is applied to conducting plates causing an active plasma region to form. The positions of substrates or wafers are shown on which the desired etching or deposition process can be affected. The geometry of the barrel type offers an obvious advantage of being volume efficient. Here the wafers can be stacked such as dominoes and the reactor

PARALLEL PLATE REACTOR



BARREL REACTOR

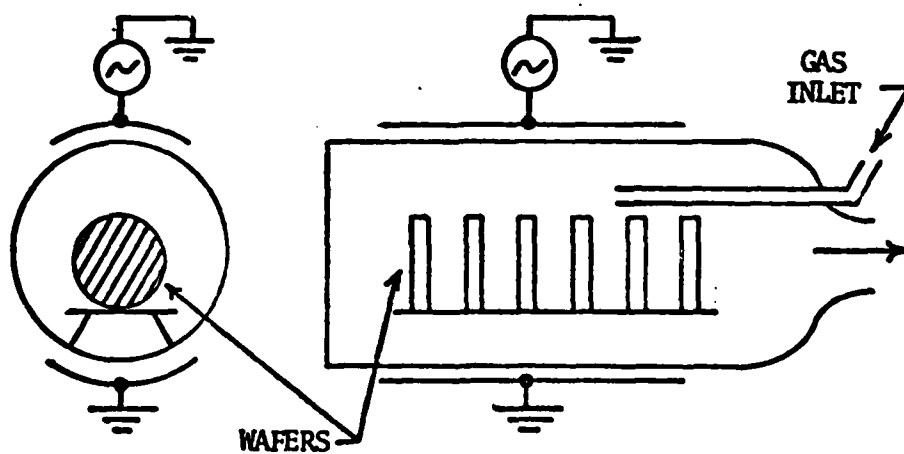


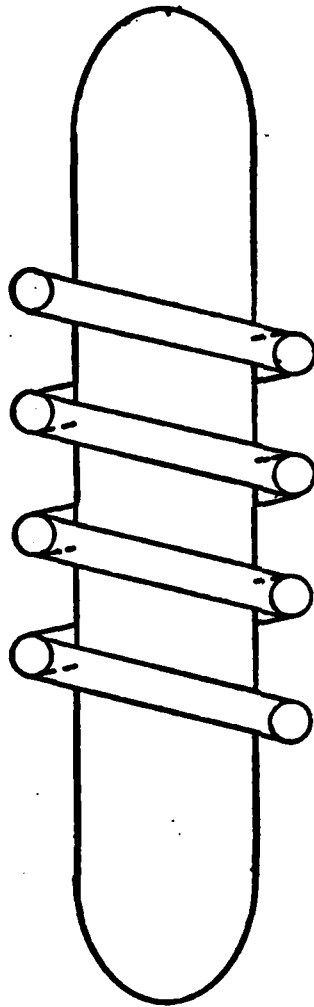
Figure 1. Plasma Reactors

designed to accommodate a large number of wafers. A high degree of uniformity results from the use of such reactors (Ilic, D.B., 1982:20). The method of RF excitation may be accomplished through a capacitive or inductive coupling. The latter finds particular use with the barrel type reactor. Figure 2 shows schematics of these alternate excitation methods. The inductively coupled reactor displays a large plasma region unobstructed by internal electrodes.

Characterization of reactor parameters in relation to the electrical driving values of frequency and power provides feedback useful in the control of plasma processes. Complicated molecular gases such as Silane (SiH_4) are often used because of their varied chemical reactions, of interest to integrated circuit technology. The level and frequency of the applied power strongly influences the energy of the electrons and this selectively determines the dissociation products produced as well as the deposition or etch rate.

The method of RF excitation, similar to driving an antenna, requires that the impedance of the load be matched to that of the circuit in order to transfer the maximum amount of power to the load. RF plasma reactors used in both research and industry have, therefore, impedance matching networks incorporated into the driving circuits to perform this function. It is possible to capitalize on this feature to make plasma measurements. Since the values of plasma parameters influence the impedance matching circuit

INDUCTIVE



CAPACITIVE

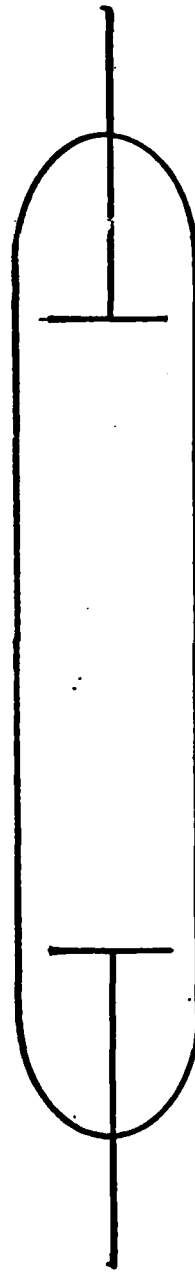


Figure 2. RF Reactors

design, it is impossible to give an all-purpose matching network for a general plasma (Norstrom, H., 1979:349). In a recent paper, H. Norstrom explains four possible classes of matching networks and selection criteria. Although the actual circuits may vary, the optimization of power transfer through impedance matching allows identification of a critical point at which measurements may be taken.

Impedance is an electrical circuit parameter. Similar to resistance, its use arises from the fact that in an AC circuit the voltage and current vary periodically and one may lead or lag the other in phase. The circuit impedance is a complex quantity consisting of both magnitude and phase information and may be expressed in polar form or converted to rectangular form to express separately a real and imaginary part. The circuit impedance can be directly measured using equipment appropriated for this experiment. Alternatively, individual circuit components can be calibrated, thereby avoiding repetitive measurements. Impedance conveys information concerning the circuit load, in this case, the plasma. By judicious measurement, impedance may be used as a plasma diagnostic. This has been demonstrated in a recent article (Ilic, D.B. 1981) where impedance techniques were developed and applied to a capacitive, parallel-plate RF plasma. In the study which follows, similar techniques are developed and applied to an inductively driven barrel-type reactor. Since the impedance measurements are performed

on existing circuitry, they have the advantage of being external to the plasma avoiding the use of traditional probes or microwave techniques and hence, are nondisturbing to particle motions or internal electric field distributions.

Problem Statement

The problem investigated in this study demonstrates that the presence of an inductive RF plasma within a barrel-type reactor interacts with the electrical driving circuit. This interaction is identified in the form of the complex impedance of a circuit element and can be used as a diagnostic to determine plasma electron number density and electron-neutral collision frequency for specified operating conditions (gas type, pressure, RF power level).

Scope and Assumptions

Study was initially conducted using a Helium plasma, chosen because of its relatively simple atomic structure, well documented collisional cross sections and its characteristically uniform behavior over wide ranges of pressure and energy. This provided a fundamental reference for development of models and evaluation of the diagnostic techniques. Time constraints did not permit a desired expansion of this study to include molecular gases such as Silane (SiH_4) which are commonly used in industrial Silicon disposition processes.

The pressure range considered was bounded by 0.01 torr at the lower limit due to the pumping capacity of the vacuum

system roughing pump. An upper bound of 1.0 torr was selected because of reported poor quality of thin films deposited at such pressures and attendant high power requirements. (Ilic, D.B., 1982:5). The plasma-generating electric field is determined by the power and frequency of the driving RF signal. The signal generator was operated over the range from 10 to 35 MHz and the amplifier permitted continuous operation at power levels up to 40 watts average power.

The spatial and temporal nature of the electric field within the plasma was not studied in detail but approaches that of a cylindrical winding with negligible end effects. This can be visualized as a uniform axial magnetic field and an azimuthal electric field, both varying sinusoidally in time. These approximations do not distort results, since impedance values are calculated from the dielectric response of the plasma. The dielectric response is a measure of the intoto response of plasma constituent particles under the influence of the applied field resulting in a net induced molecular dipole moment (Marion, J.B., 1980:23). Readers interested in a more rigorous electromagnetic field analysis are referred to Tang and his study, applicable to RF fields, using emissive probes (Tang, J.T., 1979:1458).

Two necessary models are incorporated in this study to relate the plasma to an electrical circuit measurement (the impedance). The first is formed by treating the plasma as a lossy dielectric which assigns to the plasma a complex

permittivity dependent upon plasma parameters. This is a well accepted treatment, following from electromagnetic field theory using Maxwell's equations to develop an explicit expression for a complex propagation constant. A particularly thorough analysis is given in a text written by Marr (Marr, G.V., 1968:21). The second model arises from circuit analysis when the plasma is considered as an isotropic medium contained within a circuit element.

General Approach and Organization

In the section to follow, general theory is presented to explain plasma phenomenon and establish a background for developing the mathematical relations necessary to define and quantify electrical circuit values and plasma parameters. Specific plasma parameters, electron number density, and electron-neutral collision frequency, are selected as most descriptive variables. These are investigated to determine their functional dependence upon the RF driving frequency and host gas pressure.

The specific equipment used and the physical configuration are described and shown in Figure 3. A glass barrel-type plasma tube was used with an associated low pressure vacuum system and gas supply. An impedance matching electrical network was incorporated, using an RF tunable signal generator and linear amplifier, coupled to the plasma tube with an inductive coil. A monochrometer and digital photome-

ter was available permitting spectral analysis of the emitted plasma radiation.

Procedures are developed that yield values for the plasma parameters from corresponding circuit impedance measurements. During operation, a frequency is selected, a plasma is generated, and the electrical matching network tuned to match the load impedance to that of the driving generator. Pressure and power levels are then varied while the standing wave ratio (SWR) meter is monitored to determine the impedance matching condition, that is, when maximum power is being transferred to the plasma and a minimum is being reflected back through the electrical network.

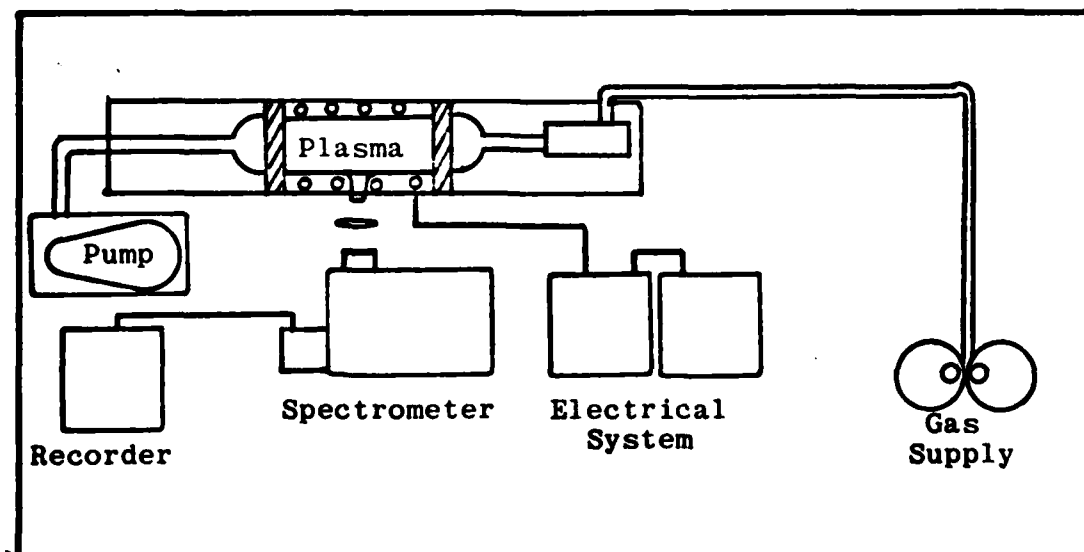


Figure 3. Equipment Layout

II. Theory

This study considers an RF generated, weakly ionized, non-equilibrium plasma. Prior to the application of the electric field, the gas contained within the reactor exists in a nearly equilibrium state. The effect of an imposed field is to cause existing free electrons (and ions), responding to a Lorentz force, to gain kinetic energy. The presence of neutral particles, unaccelerated by the field, inhibits electron motion and facilitates energy transfer among particles. As the electrons attain energies sufficient to overcome ionization thresholds during collisions, a plasma is generated. For any given level of driving power, a steady state is reached where the energy and particle losses from diffusion, recombination and radiation balance the energy being absorbed by the plasma from the field. Implicitly, particle collisions perform a controlling function in both the electron production and loss mechanisms occurring within the plasma.

The effect of an alternating electric field on a free electron is to cause the electron to oscillate within limits of velocity and kinetic energy determined by the field strength and period. Over time the electron will not gain energy from the field under these conditions. In the presence of other particles, however, resulting collisions redirect the motions, allowing the electrons to accumulate random, thermal energy.

If the applied electric field is sinusoidally varying in time and expressed as: $E(t) = E \cos \omega t$, the rate energy is gained from the field can be approximated by:

$$\frac{dE}{dt} = \frac{e^2 E^2}{2m} \frac{v}{(\omega^2 + v^2)} \quad (1)$$

(Stamm, M.R., 1981:26)

where e and m are the electron charge and mass respectively, E is the field amplitude, ω , the driving frequency and v , the collision frequency.

The collision frequency is important because it also appears in energy and particle loss terms. The rate of free electron production is directly related to the rate of energy shown and thus dependent explicitly on the collision frequency. Two limiting cases may be considered. In the DC approximation ω approaches zero and the rate of production scales inversely with the collision frequency. In this instance the mechanism may be thought of as an electron being accelerated by the field, suffering a collision resulting in the exchange of its energy, then being reaccelerated until subsequent collisions. The distance between collisions is termed the mean free path and the rate of collisions, the collision frequency. Clearly, the occurrence of collisions acts to impede the progress of the electrons to some limiting velocity, termed the drift

velocity.

In the case where the electric field is rapidly oscillating, ω is much greater than the collision frequency and the rate of production depends directly upon the rate of collisions but is strongly inversely dependant upon the driving frequency. Each of these limits must be considered in this experiment since the operating ranges of control parameters (gas pressure, power, frequency) place the driving frequency-collision frequency relationship within the transition between these two regions. In the absence of compensating effects, experimental data can be expected to reflect the effects of this transition between adjoining regimes.

Because of their more rapid response to the applied field, it is the electrons rather than the ions which drive plasma processes. The rate at which energetic electrons stimulate particular reactions is best contemplated by assigning to each collisional event a specific cross section which implicitly relates the probability of occurrence to a function of the average energy of the electron. For molecular gases, energy dependant electron impact cross sections are often very complicated functions. Fortunately, the choice of Helium for a constituent gas, provides a relatively complete set of collision cross sections. Electron excitation and ionization cross sections for Helium have been accurately measured as functions of electron energy

and comprehensive data is readily available therefore it is not necessary to repeat here. (Brown, S.C., 1966:133)

Electrons below inelastic energy thresholds suffer only elastic collisions with the molecules. As the electrons gain kinetic energy and excitation/ionization thresholds are reached, inelastic collisions occur causing radiative losses through excitation/de-excitation events and the electron population increases through ionizations. As the electron number density grows, a characteristic plasma glow is observed. Since the available power level is limited, balancing loss mechanisms limit fractional ionization levels in this experiment to the order of 10^{-2} .

From this discussion, it is apparent that the rate of plasma generation is determined by the electron number density and the frequency of collisions. The collision frequency is expressed as the electron velocity divided by the mean free path. This can be related to the cross section as:

$$v = v n \sigma \quad (2)$$

(Chen, F.F., 1977:137)

where v is the electron velocity, n is the neutral particle number density and σ is the electron impact cross section. The neutral particle number density is a function of host gas pressure. The mean electron velocity can be expressed

in terms of energy and the collision frequency then written:

$$\nu = B p \sigma T_{ev}^{\frac{1}{2}} \quad (3)$$

(Hirsh, N.H., 1928:177)

where T_{ev} is energy in electron volts, p is gas pressure in torr, σ is the cross section and B is a proportionality constant equal to 21.0×10^{25} for these units.

For select atomic gases, including Helium, the collision frequency is found to be relatively constant over a broad range of energy. Hydrogen also belongs in this group but its use was considered too volatile. Heg, a mixture of Helium and mercury belonging to this category was unavailable. Brown has compiled measurements of these gases and gives the result for Helium as:

$$\nu = 2.37 \times 10^9 p \quad (4)$$

(Brown, S.C., 1966:168)

Electron losses are also controlled by the collision frequency. Random motion caused by the thermalizing effect of collisions bring particles to the container walls where they recombine. In addition to this "free diffusion", the collective behavior of the plasma introduces ambipolar diffusion in that the higher mass of the ions and attendant slower response inhibit the electron diffusion. If the

electrons and ions were to diffuse, each at its own free diffusion rate, the net charge difference would continue to grow over time. Instead, the plasma responds by establishing internal fields so as to reduce the electron flux and increase the ion flux until both species diffuse at the ambipolar rate. Ambipolar diffusion dominates in plasmas that have physical dimensions that are large compared to the Debye length. In this experiment, the Debye length is on the order of a millimeter, much less than the tube diameter of 10 cm.

The effect of ambipolar diffusion is to increase the ion diffusion rate by a factor approximating the ratio of the ion to electron energy (Stamm, M.R., 1982:35). We will consider a factor of 40 to be appropriate here. The coefficient of diffusion is approximated by the following expression:

$$D = \frac{\bar{v}\lambda}{3} = 5 \times 10^3 \frac{\lambda T_{ev}^{\frac{1}{2}}}{A^{\frac{1}{2}}} \quad (5)$$

(Stamm, M.R., 1982:48)

where A is the atomic weight in atomic mass units and the remaining quantities are as previously defined. For a 1 torr Helium plasma at 300° K with a cross section of $5 \times 10^{-14} \text{ cm}^{-2}$, the ambipolar diffusion coefficient is calculated to be $100 \text{ cm}^2/\text{sec}$ (Stamm, M.R., 1982:50).

This is in agreement with experimental data (Brown, S.C., 1967:128). The time for diffusion can be written in terms of a characteristic diffusion length:

$$\frac{1}{\tau} = \frac{D}{\Lambda^2} \quad (6)$$

(Stamm, M.R., 1982:44)

The diffusion length is based on the geometry of plasma container and is found by solving Laplace's equation for the steady state case. For a cylindrical geometry it is found to be:

$$\frac{1}{\Lambda^2} = \left(\frac{\pi}{L} \right)^2 + \left(\frac{2.405}{R} \right)^2 \quad (7)$$

(Hirsh, M.N., 1978:188)

Applying the above to this experiment gives a value for Λ of 2.07 and a time for diffusion of 0.04 sec.

The relatively slow response of the ions introduces another important effect which impacts the ability of the electric field to sustain the plasma and causes frequency dependant behavior in the plasma parameters. Initial displacement from an electron-ion equilibrium position results in a restoring force. Particle inertia causes restoring particle motions to overshoot the equilibrium positions, giving rise to an oscillation which occurs at a character-

istic frequency. By expressing the particle motions as an equation of motion and applying Maxwell's equations, the plasma frequency, ω_p , is found to be:

$$\omega_p = \left(\frac{4\pi n e^2}{m} \right)^{\frac{1}{2}} \quad (8)$$

(Chen, F.F., 1977:73)

Noting the dependence on the electron number density, it is convenient to combine the constants and use the following approximation:

$$f_p = 9000 n^{\frac{1}{2}} \quad (9)$$

(Chen, F.F., 1977:73)

Maxwell's equations also leads to a dispersion relation for transverse electromagnetic waves propagating through a plasma. Considering a simple case where there are no external magnetic fields imposed, the dispersion relation can be written in terms of a propagation constant, K , and the velocity of light, C , as:

$$K^2 = \frac{1}{C^2} (\omega^2 - \omega_p^2) \quad (10)$$

(Chen, F.F., 1977:102)

The salient feature of this relation is that the

propagation constant becomes imaginary when the wave frequency exceeds the plasma frequency. Stated another way; when the plasma frequency is fixed, due to a specified number density, electromagnetic waves below the plasma frequency will not propagate through the plasma. For a density of 10^{10} cm^{-3} , the plasma frequency is on the order of a gigahertz. This explains the wide use of microwave radiation for plasma study.

At frequencies below the plasma frequency the extent of penetration of the electromagnetic radiation is limited. A measure of the depth of penetration is termed the skin depth, δ , which describes the distance required for the radiation to be attenuated to $1/e$ of its initial value and obeys the following relation:

$$\delta = \frac{C}{(\omega_p^2 - \omega)^{1/2}} \quad (11)$$

(Chen, F.F., 1977:103)

Here C is the velocity of light and other terms are as previously defined. This indicates that at all frequencies below the plasma frequency there is finite penetration.

This discussion presents a paradox when applied to the RF case of study. It would appear that the RF energy being used to generate the plasma would not be allowed to penetrate the boundary once the plasma was formed to sustain the

discharge. Although this holds true for the proper boundary conditions, in this experiment, the dimensions of the plasma (10 cm) are small compared to the free space wavelength (15 meters), (Sanders, S.G., 1978:2690). With this consideration and allowing for a finite skin depth, sufficient penetration is made to sustain the discharge (Marion, J.B., 1980:151).

This discussion again points out the importance of the particle density. This parameter acts to balance the free electron-ion production caused by the field with the losses due to diffusion to and recombination at the container walls by controlling collisions.

During operation, the plasma is formed and allowed to stabilize before measurements are taken. In this steady state, the rate of free electron losses must equal the rate of production. The equation of continuity is:

$$\frac{dn}{dt} = n n_a R_I - \frac{D}{\Lambda^2} n - \alpha n^2 \quad (12)$$

In the first term, n_a is the neutral gas number density and R_I is the average rate of ionization found by summing individual ionization rates from the ground and excited state collisional events. The second term considers losses from diffusion as previously discussed. The third term is included to account for volume recombination events. Since this term is non-linear with respect to electron number density,

the equation of continuity can be solved in the steady state, for the number of free electrons in the plasma. This becomes:

$$n = \frac{1}{\alpha} \left(n_a R_I - \frac{D}{\Lambda^2} \right) \quad (13)$$

An increase in driving power level causing an increase in the production rate of ionizations is shown by the above expression to imply an increase in number density. This trend is an expected observation in the experimental data.

It is necessary to relate the plasma parameters to the electrical circuit in order that electrical measurements will yield meaningful information about the collision frequency and number density. This linkage is affected by modeling the plasma as a lossy dielectric with a permittivity explicitly described by the plasma parameters. The complex permittivity is given by either of the following two expressions:

$$\epsilon_p = \frac{\omega_p^2}{\omega^2 - i\nu\omega} \quad (14)$$

(Ilic, D.B., 1981:1544)

$$\epsilon_p = 1 - \frac{\alpha m}{\omega^2 + \nu^2} - i \frac{\alpha \nu m}{\omega(\omega^2 + \nu^2)} \quad (15)$$

where α is a numerical constant arising from the dependence of the plasma frequency on number density and equals 3182

in MKS units. Other variables are as previously defined. The second equation is in rationalized form delineating the real and imaginary parts of the function.

The plasma permittivity can be incorporated into expressions for a measurable circuit parameter, the impedance. The impedance is also represented by a complex number although for purely capacitive or inductive circuit components, the expressions are pure imaginary numbers. If the lossy dielectric plasma is considered to be the medium within a circuit capacitor, the resulting capacitance is found from the basic air-gap capacitance by using the permittivity as a proportionality expression. The product of the imaginary portion of the plasma permittivity with the imaginary capacitive impedance produces an additional real term analogous to resistive components.

The impedance may be given in polar form thereby carrying magnitude and phase information. This is a more usable form when impedance matching is considered since the desire here is to maintain continuity of phase between the circuit and load. Polar form was also compatible with the available measurement equipment.

Circuit Model

The model chosen to represent plasma-circuit relationships is dependant upon the reactor geometry and type. In the simplest case of the capacitive type parallel-plate

reactor investigated by Ilic, the plasma fills the volume between the plates and the capacitance is given by the expression: $C = e_p C_o$, where C_o is the basic capacitance of the reactor determined geometrically from the area and separation of the parallel plates. (Ilic, D. B. 1981:1544) It follows immediately that the reactor impedance is given by:

$$Z_p = \frac{1}{i\omega e_p C_o} \quad (16)$$

In the case of the inductively excited barrel reactor used in this experiment, the circuit model is more involved. Here the value of the basic capacitance cannot be determined geometrically. With this in mind, the model chosen to represent the plasma-circuit relationship is that of a capacitor in parallel with the driving inductor. For generality, the total capacitance associated with the inductor is separated into components and accounts for the effect of parasitic capacitance as well as plasma effects. Figure 4 shows schematically the plasma model and its relationship to the driving circuit. As shown, L represents the inductor, C_B , the portion of the parasitic capacitance unaffected by the plasma and C_o , the capacitance interior to the plasma tube which is modified by the presence of a plasma of relative permittivity, e_p . For this analysis, the plasma-circuit model is treated as an unknown impedance, Z_p . When combined

with the driving inductor, the circuit reduces to an equivalent impedance, Z_e , at the point in the circuit where measurements are to be extracted.

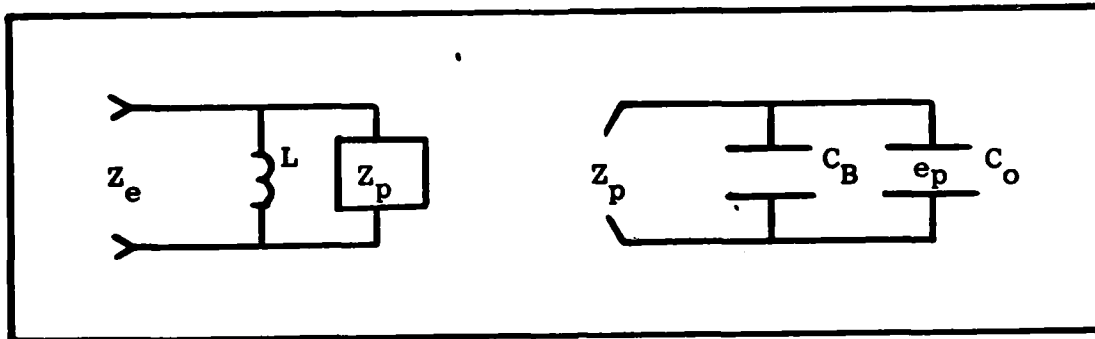


Figure 4. Plasma Model

The expression for the impedance of this model is:

$$Z_p = \frac{1}{i\omega(C_B + e_p C_o)} \quad (17)$$

The analysis appropriate to each of the above models differs only slightly, however the parallels drawn are significant. The analysis of the capacitive case can be gleaned from a critical review of Illic's study. In this article, Illic presents a method of determining electron-neutral collision frequency and electron number density in a capacitive type plasma reactor. Mr. Illic did not address an equally important class of plasma reactors, that of the inductive type. The question of whether this method, with

some modification, could be extended for use with an inductive type plasma reactor suggested the investigation presented in the body of this thesis. Since motivation for much of the analysis stems from parallel arguments, more than a cursory summary of this reference is warranted.

It must be emphasized that the method presented was applied to capacitive type reactors only and indeed is applicable only to a particular subset requiring a maximum energy transfer into the plasma. This requirement is satisfied when a SWR of 1.0 is established. The plasma reactor is treated as an electrical circuit element for analysis. The other essential elements are the RF signal generator and matching network. When the matching network is properly tuned, the imaginary part of the complex impedance vanishes and the signal generator drives a known, purely resistive load.

The matching network consists of two variable capacitors and an inductor. The plasma load is also capacitive. Using traditional circuit analysis, the electrical components are reduced to an expression for a single complex impedance based on the values of the individual circuit elements which are then measured or determined from calibrated curves.

Choosing the plasma lossy dielectric model with permittivity given by Equation (14) and using Equation (16), the impedance can be rewritten as:

$$Z_p = \frac{(\omega^2 - i v \omega)[v \omega - i(\omega^2 - \omega_p^2)]}{\omega C_o [(\omega^2 - \omega_p^2)^2 + v^2 \omega^2]} \quad (18)$$

The numerator can be expanded and simplified into the form:

$$\text{Numerator} = \omega[v \omega_p^2 + i \omega(\omega_p^2 - \omega^2 - v^2)] \quad (19)$$

Similarly, the denominator gives the form:

$$\text{Denominator} = \omega^5 C_o \left[\left(\frac{\omega_p^2}{\omega^2} - 1 \right)^2 + \frac{v^2}{\omega^2} \right] \quad (20)$$

Writing the impedance in rectangular form gives a real and imaginary component such that $Z_p = R_p + iX_p$. Also, a factor G is defined in the following manner:

$$G = \left(\frac{\omega_p^2}{\omega^2} - 1 \right)^2 + \frac{v^2}{\omega^2} \quad (21)$$

This mathematically arbitrary but convenient form allows simplified expressions for the impedance. The components are as follows:

$$R_p = \frac{v \omega_p^2}{\omega^4 C_o G} \quad (22)$$

$$X_p = \frac{\left(\frac{\omega_p^2}{\omega^2} - \frac{v^2}{\omega^2} - 1 \right)}{\omega C_o G} \quad (23)$$

These components yield an impedance from values of plasma parameters. Our desire is to do the inverse, that is, knowing the value of impedance, discern the value of plasma quantities. We note that the equations are coupled and therefore solving for explicit expressions of plasma parameters is tedious. Again an arbitrary choice is made and a new quantity, H , is defined by:

$$H = R_p^2 + X_p^2 + \frac{X_p}{\omega C_0} \quad (24)$$

Careful examination of the expression R_p , solved for ν , reveals that this factor H must also obey the following:

$$H = \frac{\omega_p^2}{\omega^2 C_0^2 G} \quad (25)$$

Although not immediately apparent, several intuitive substitutions can show that the above two expressions lead to an identity. In the process of performing this critical step, an explicit expression for collision frequency arises. Further manipulation yields an expression for plasma frequency which we recall is dependant upon number density. The final expressions for these parameters, in agreement with Illic's study, are the following:

$$\nu = \frac{R_p}{C_0 H} \quad (26)$$

$$n = \frac{\omega^2}{3182} \left[1 + \frac{(X_p + \frac{1}{\omega C_o})}{\omega C_o H} \right] \quad (27)$$

The experimental aesthetics of this method arise from the realization that once calibration curves for the circuit components are determined, plasma collision frequency and number density can be calculated from the matching network counter readings. This is particularly convenient for the configuration presented in this article which embodied an automatic tuning network.

Mr. Ilic presented one example to verify that reasonable values could be obtained for a Nitrogen discharge driven at a frequency of 13.56 MHz. Lack of a more dynamic range encourages further investigation. Variable components were measured at low frequency which makes wider application somewhat suspect unless considerable attention was given to eliminating stray capacitive effects. Even small unaccounted-for values of inductive-capacitive coupling introduce significant increases in apparent component values as studied by R. A. Olsen and observed by this thesis student (Olsen, R.A., 1961:2). Collision frequency is determined from a resistive term which arises from the presence of the imaginary term in the expression for the plasma permittivity. The magnitude of this resistive term is small and demands high measurement accuracy to infer an associated collision frequency.

Returning to the case under investigation in this study,

a parallel development can be performed. Using the same expression for permittivity and the expression for the impedance applicable to the inductive barrel-type reactor, the combination gives the following:

$$Z_p = \frac{(\omega^2 - i\nu\omega)}{\omega^2 C_o \left[\nu \left(1 + \frac{C_B}{C_o}\right) + i\omega \left(1 + \frac{C_B}{C_o}\right) - \frac{\omega_p^2}{\omega^2} \right]} \quad (28)$$

For convenience, a numerical constant γ is defined as:

$$\gamma = 1 + \frac{C_B}{C_o} \quad (29)$$

By redefining the term G used previously, the impedance can again be expressed in component form. Let:

$$G = \left(\frac{\omega_p^2}{\gamma\omega^2} - 1 \right) + \frac{\nu^2}{\omega^2} \quad (30)$$

It is instructive to compare the above expression to that pertaining to the capacitive case, Equation (21) and note the inclusion of the constant, γ . Likewise, the term appears in the following expressions:

$$R_p = \frac{\nu\omega_p^2}{\omega^4 \gamma^2 C_o G} \quad (31)$$

$$X_p = \frac{(\frac{\omega_p^2}{\gamma\omega^2} - \frac{v^2}{\omega^2} - 1)}{\omega\gamma^2 C_o G} \quad (32)$$

Again we wish to solve for the plasma parameters and with the same justification as before, we define a new H, such that:

$$H = \gamma R_p^2 + \gamma X_p^2 + \frac{X_p}{\omega C_o} \quad (33)$$

This selection gives, after some careful manipulation, the sought after expressions which explicitly relate the collision frequency and number density to measured impedance values. These relations are:

$$v = \frac{R_p}{C_o H} \quad (34)$$

$$n_e = \frac{\omega^2}{\alpha} \left[\gamma + \frac{(\gamma X_p + \frac{1}{\omega C_o})}{\omega C_o H} \right] \quad (35)$$

In the above, α is a constant arising from the conversion from plasma frequency to collision frequency ($\alpha = 3.182 \times 10^9 \text{ cm}^3/\text{sec}^2$). It remains to determine numerical values for the real and imaginary parts of the plasma impedance. This is accomplished through measurements of the inductor, L, and the equivalent impedance, Z_e . Circuit analysis reduces Z_p to the following expression:

$$Z_p = \frac{-\omega L X_e + i\omega L R_e}{-R_e + i(\omega L - X_e)} \quad (36)$$

A value for L was found to be 2.70 microhenrys. The expression for Z_p can be rationalized to give the real and imaginary parts, however, the present form is usable in a subroutine of a computer program which is used for data reduction. (See Appendix C).

III. Equipment

The equipment employed in the study is discussed under the following functional categories: Plasma tube, vacuum system, electrical system, optical system, and an overall configuration.

Plasma Tube

The plasma tube diagrammed in Figure 5 is a locally fabricated, low pressure, pyrex glass tube having a diameter of 10 cm and a length of 56 cm. The tube incorporates opposing input-output openings to provide a non-turbulent gas flow, a pressure port, and a viewing tube and window. Two similar plasma tubes were used. One without a viewing tube was used for study of atomic gases; the second, includes the viewing tube provision which is necessary to prevent contamination of the viewing window by RF deposition when molecular gases such as Silane are studied.

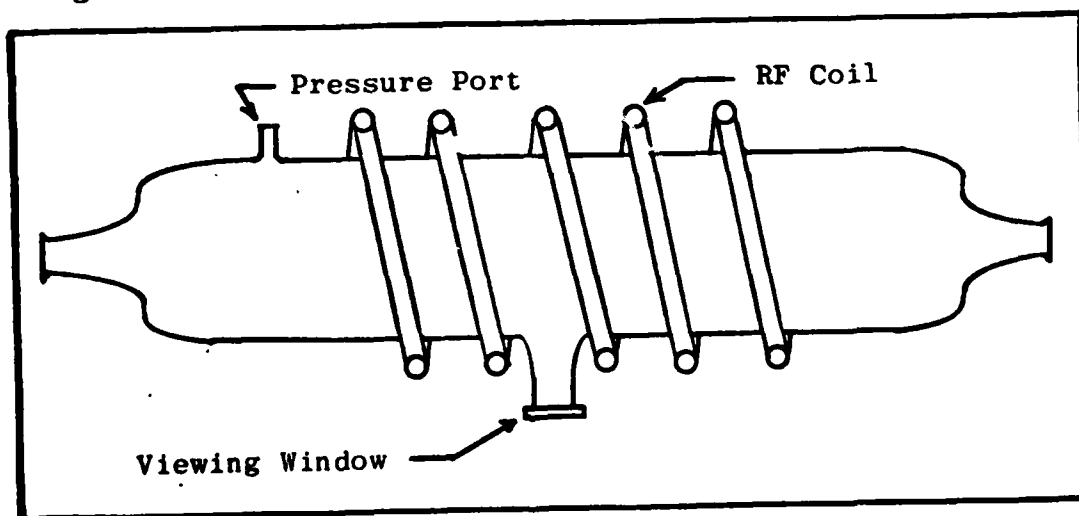


Figure 5. Plasma Tube

Vacuum System

The vacuum system utilizes a DuoSeal, Model 1397, low-vacuum mechanical pump. Positive shutoff valves, controllable flow valves, mixing manifold and associated flow meters and pressure gauges control the flow and content of the gas contained within the plasma tube. Provisions are made to dilute the vacuum pump exhaust thereby avoiding possible volatile reactions which can occur between ambient air and molecular gases such as Silane. Since this experiment uses a flowing gas system, the roughing capacity of the vacuum pump establishes a practical lower pressure limit of 0.01 torr. The vacuum system is shown schematically in Figure 6.

The gas under investigation flows from bulk gas supply cylinders through a pressure regulator which is adjusted to maintain a pressure consonant with downstream meters and valves (approximately 10 psi). The gas passes through a calibrated chamber where a transducer is used to determine an accurate volume flow rate. The gas then passes through a glass flow tube providing a secondary flow rate reading. Controllable flow valves and positive shutoff valves admit the desired flow into a manifold which stabilizes the flow into the plasma tube. A direct reading pressure gage, readable to one torr, provides approximate system pressure. A pressure sensor calibrated for the specific gas under study is connected close to the active plasma region to give accurate readings down to 10^{-4} torr. Exhaust is expelled

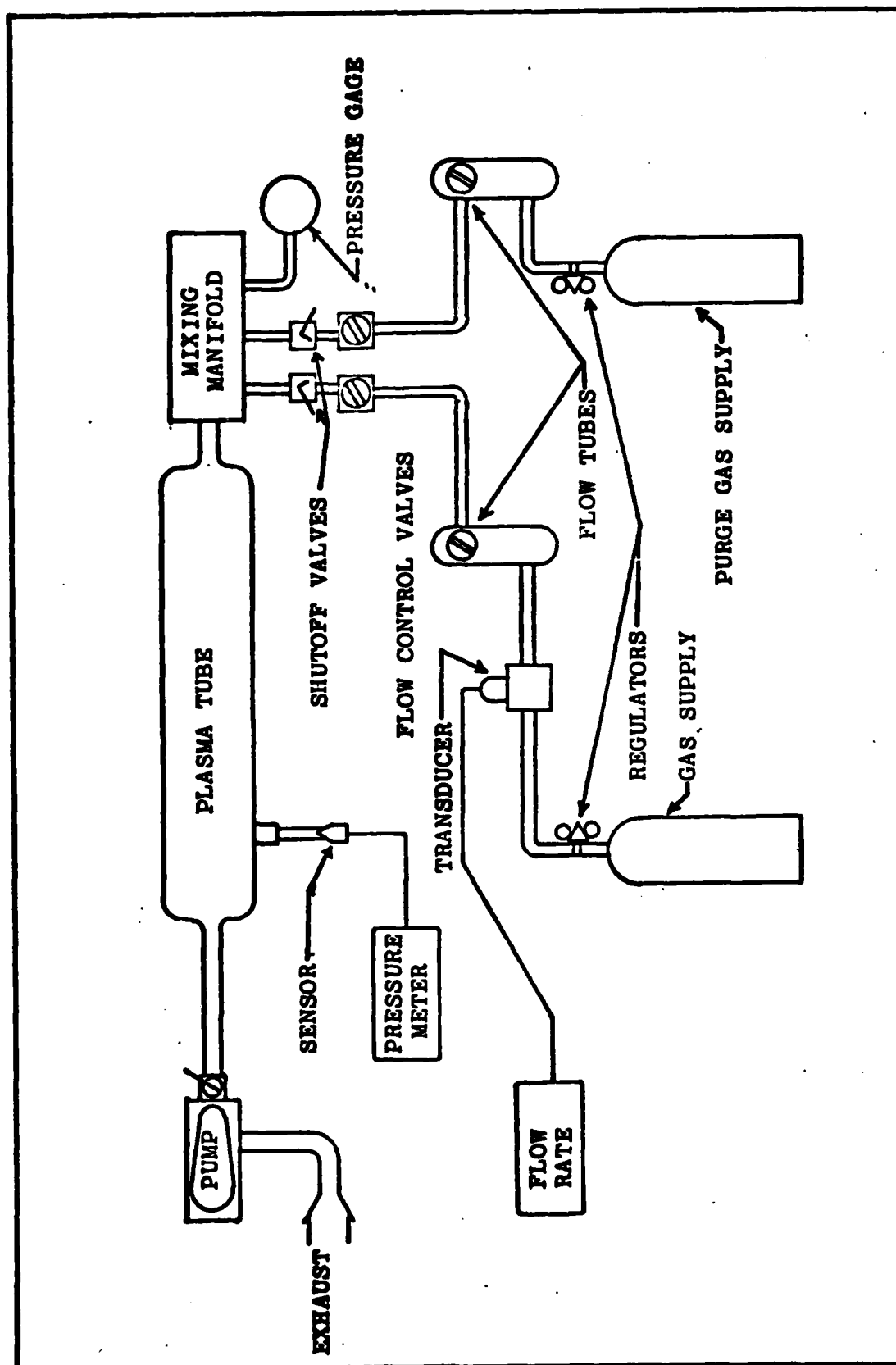


Figure 6. Vacuum System

through a constant volume vacuum pump and diluted to ambient.

Electrical System

The electrical system makes use of a Hewlett Packard, Model 606A, RF signal generator, a Hewlett Packard, Model 5245L, digital frequency counter, a Heathkit, Model 2040 antenna tuner, a linear amplifier, and associated meters to deposit RF energy into the plasma by means of an induction coil. A component demanding stringent specifications for this experiment is the linear amplifier. The Amplifier Research, Model 40L, linear amplifier employed here incorporates unique circuitry which allows operation into any load impedance. This is critical, since plasma generation introduces an unknown impedance and a prolonged mismatched condition often exists until the tuning procedure can be accomplished and measurements taken.

An HP 4815 RF Impedance, Vector Voltmeter was used for calibration and impedance measurements. Figure 7 shows the electrical system components. The tuner is shown expanded and labeled: "matching network", because of its importance in circuit analysis.

Optical Diagnostic System

A SPEX Model 1870 Czerny-Turner Spectrograph provided a means of correlating emission spectra to calculated plasma parameters. The spectrometer with associated variable scanning drive, digital photometer, photomultiplier and cooling

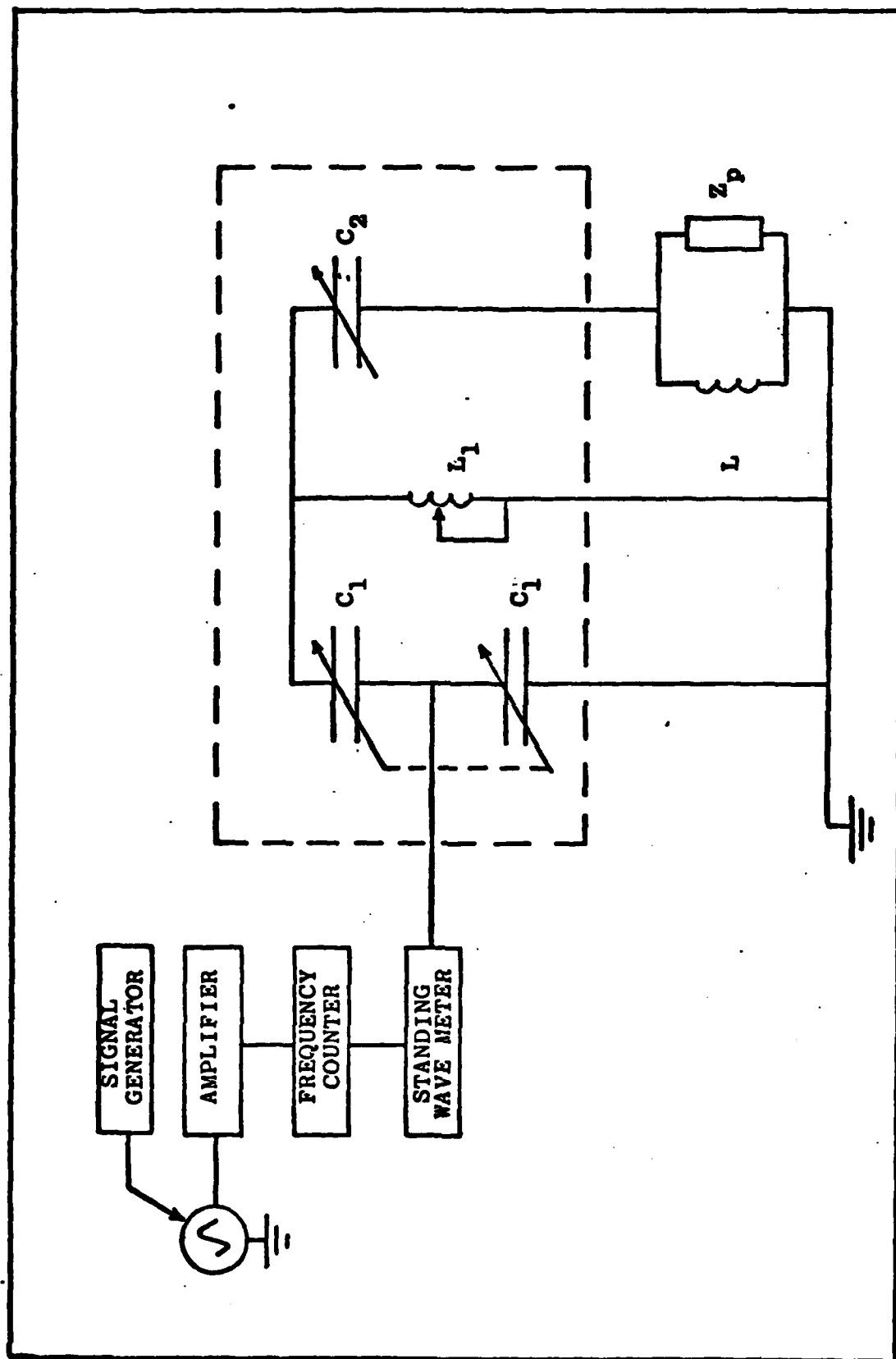


Figure 7. Electrical System

system, and strip chart recorder is coupled to the plasma tube with a choice of optical doublets. The spectrometer has an $f/\#$ of 8.6, entrance and exit slit widths variable from 0 to 3 mm and a choice of three slit heights. Because of limited table space, an appropriate input doublet was procured corresponding to each slit height to focus the plasma emission onto the entrance slit without the need for changing overall object to image distance. In each case, the input optics would slightly overfill the slit to provide maximum throughput with minimum background interference. Figure 8 shows the input optics relationships.

Configuration

The overall equipment configuration is shown in Figure 9. The plasma tube complete with mixing manifold was mounted on a platform designed for ease of alignment relative to the spectrometer. The electrical system is coupled to the plasma tube via the induction coil. The optical system is coupled through the input optics. The plasma tube and driving coil were enclosed within a grounded aluminum cage. External coaxial electrical connections were added to facilitate impedance measurements.

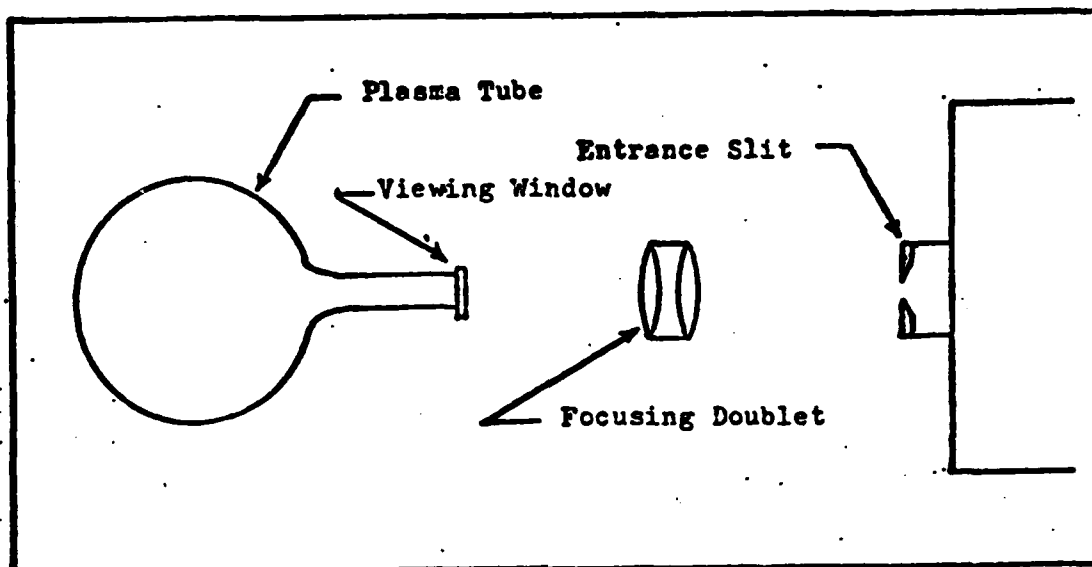


Figure 8. Optical System

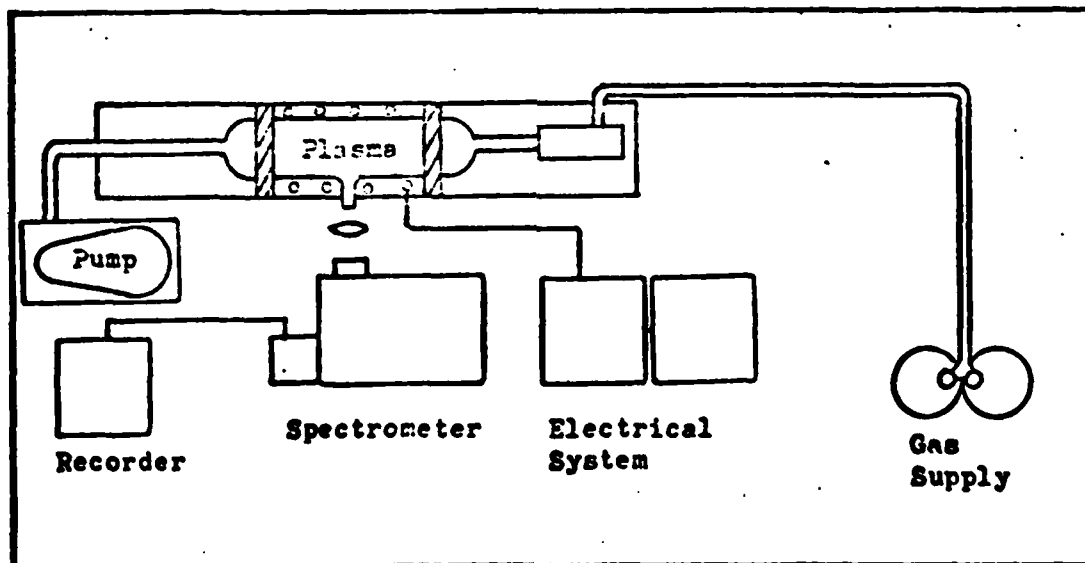


Figure 9. Equipment Layout

IV. Procedure

Impedance measurements were taken using the following procedure. With the vacuum pump maintaining a constant-volume pumping rate, the flow control valve was adjusted to establish a desired pressure within the plasma tube. The frequency of interest was selected on the signal generator and RF impedance meter. Both were calibrated using the digital frequency meter to assure equivalence. The power level of the amplifier was raised to produce a plasma. If a plasma was not readily generated due to a highly mismatched condition, the matching network was readjusted. Once a plasma was generated, and an approximate forward power level established, the Standing Wave Ratio (SWR) meter was monitored while the matching network was tuned to a SWR of 1.0.

The actual matching procedure is dependant upon individual load parameters. The tuner has three variable components but no consistent order of adjustment was universally productive. However, familiarity reduced tuning time considerably. In tuning an unknown impedance, the most reliable procedure was to reduce the sensitivity of the SWR meter to keep an on-scale reading, adjust the tuner inductor until a slight dip was observed in the SWR, then position both capacitors for a minimum SWR and then, alternately increment the inductor and the antenna matching capacitor while checking for a lower minimum SWR reading after each pair of adjustments.

Once a SWR of 1.0 was attained, a measurement could be taken.

With the amplifier positioned to standby, the coaxial cable was removed from its connector at the driving coil. The impedance of the aggregate of forward components was measured at this point and labeled Z_{cable} . Since the impedance was matched (SWR = 1.0), the equivalent impedance of the coil and plasma, Z_e , adds vectorally with the value of Z_{cable} to produce a zero phase condition. Thus, if we measure Z_{cable} in polar form, Z_e must necessarily be of the same magnitude and opposite phase. This value of Z_e is then used in appropriate theoretical equations to determine collision frequency and number density. The following figure indicates this measurement schematically.

The value of the driving inductor, L ., was determined from a resonance condition. The inductor has an associated interturn capacitance, C , and the combination can be treated as a capacitor-inductor parallel circuit having an impedance

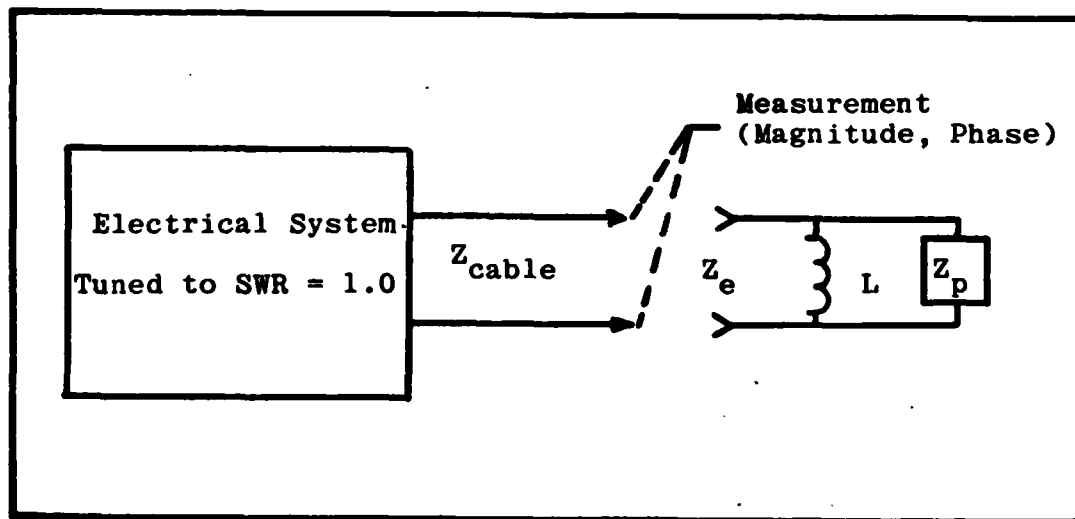


Figure 10. Impedance Measurement

given in magnitude by:

$$|Z| = \frac{\omega L}{1 - \omega^2 LC} \quad (37)$$

By making an impedance measurement at several different frequencies, the value of L was found to be 2.70 microhenrys and C was found to be 9.5 picofarads.

As discussed in Section II, the capacitance measured above was considered to consist of an internal and external component. The sensitivity of the measurements requires that the capacitance be accurately apportioned between its components. This was accomplished by taking impedance measurements with each of two different dielectric materials filling the plasma tube. The first material was dry air having a dielectric constant of unity. The second material was carbon tetrachloride which was chosen for its dielectric constant of 2.27. This value is essentially invariant to frequency changes over the RF range. Since the presence of the dielectric influences the internal capacitance only, these measurements allow for solving simultaneously for the values of the individual capacitances. The internal capacitance, C_0 , was found to be 0.52 pf and the external capacitance, C_B , 8.98 pf.

V. Results

Plasma-Circuit Interaction

The thrust of this thesis is to infer the magnitudes of plasma parameters from their effect upon electrical circuit elements, in particular, the driving inductor. The fact that the presence of a plasma does have detectable impact was demonstrated conclusively. By generating a plasma and tuning the matching network, a SWR of 1.0 was attained, indicating a matched impedance load. After extinguishing the plasma (by momentarily interrupting the power at below threshold levels), a substantial deflection was noted on the SWR meter. This indication of a mismatched condition, the plasma's effect, encouraged attempts to quantify the plasma-circuit perturbation through impedance measurements.

Model Validation

The basic model chosen for analysis is that of a theoretical plasma-filled capacitor connected, in parallel, to the driving inductor. This model was shown to have some validity through the following experiment.

A variable capacitor was installed in a parallel position to the driving coil to allow simulation of the plasma. When the plasma was extinguished, corresponding to a change in the theoretical plasma filled capacitor, the SWR meter deflected substantially from its annulled reading.

The impedance matched conditon could be restored by making a small adjustment (approximately 2 picofareds) on the variable capacitor. Thus, changes in a real, physical capacitor, in parallel, duplicate observed phenomena attributed to plasma parameters. The converse suggests that the same effects can be attributed to a theoretical, plasma-filled capacitor in the same parallel configuration.

Application

Measurements were made of the circuit impedance as a function of pressure and power using procedures outlined in Section IV. The data was reduced using equations presented in Section II and Appendices B and C. The resulting plots were then examined for possible trends which would correlate to the theory discussed in Section II. Figures 11 through 14 present examples of the measurements taken. The quantity being measured is complex and the meter readings are given in polar form. Each measurement gives two points of information, a phase angle and a magnitude. Plotting the data in polar form was found to be awkward for interpretation therefore, each measurement was converted to rectangular form. This allows the real and imaginary parts of each measurement to be plotted individually. Although the data is plotted on separate graphs, the real and imaginary portions must be understood to be coupled in order to maintain proper perspective.

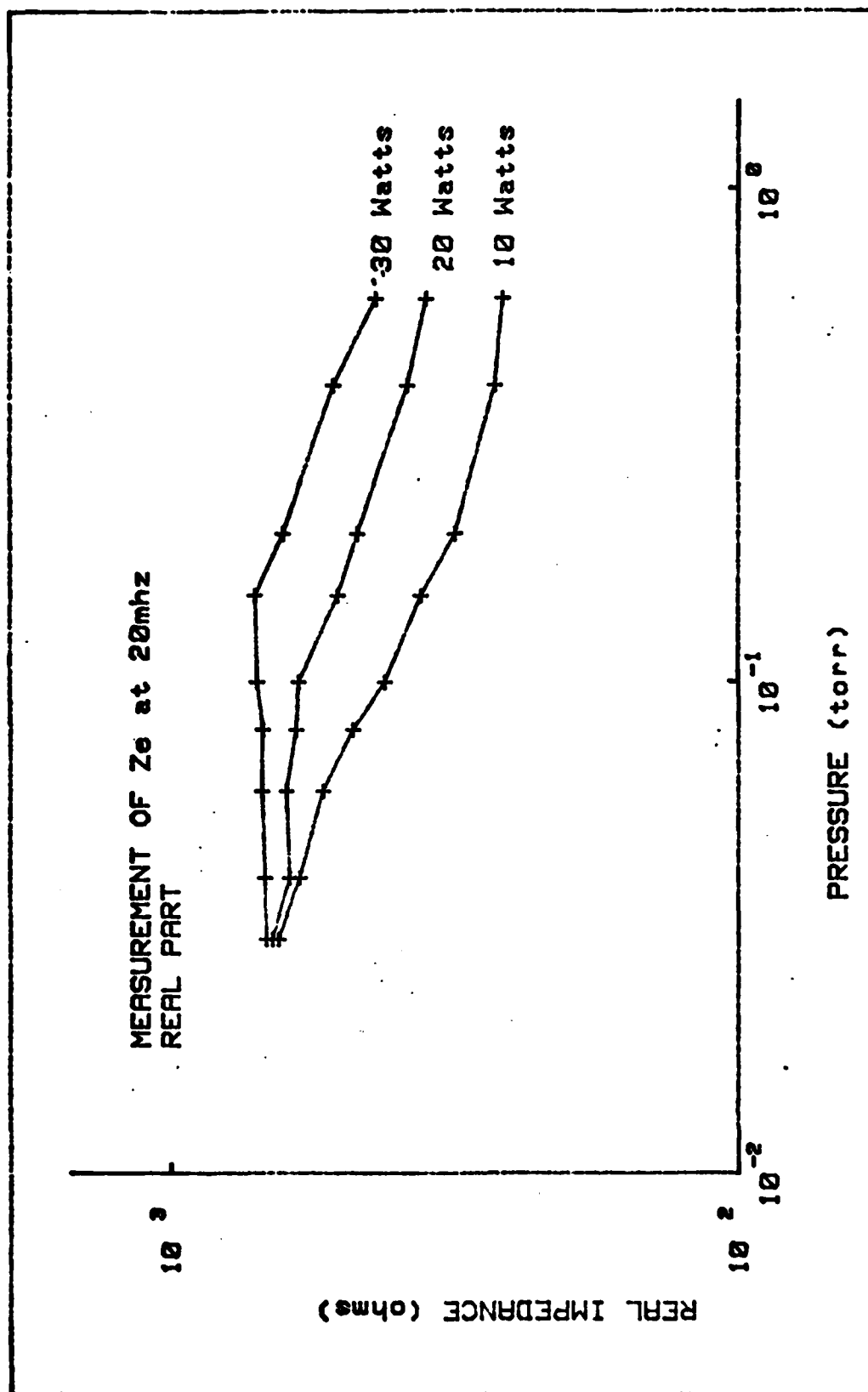


Figure 11. Real Impedance Component

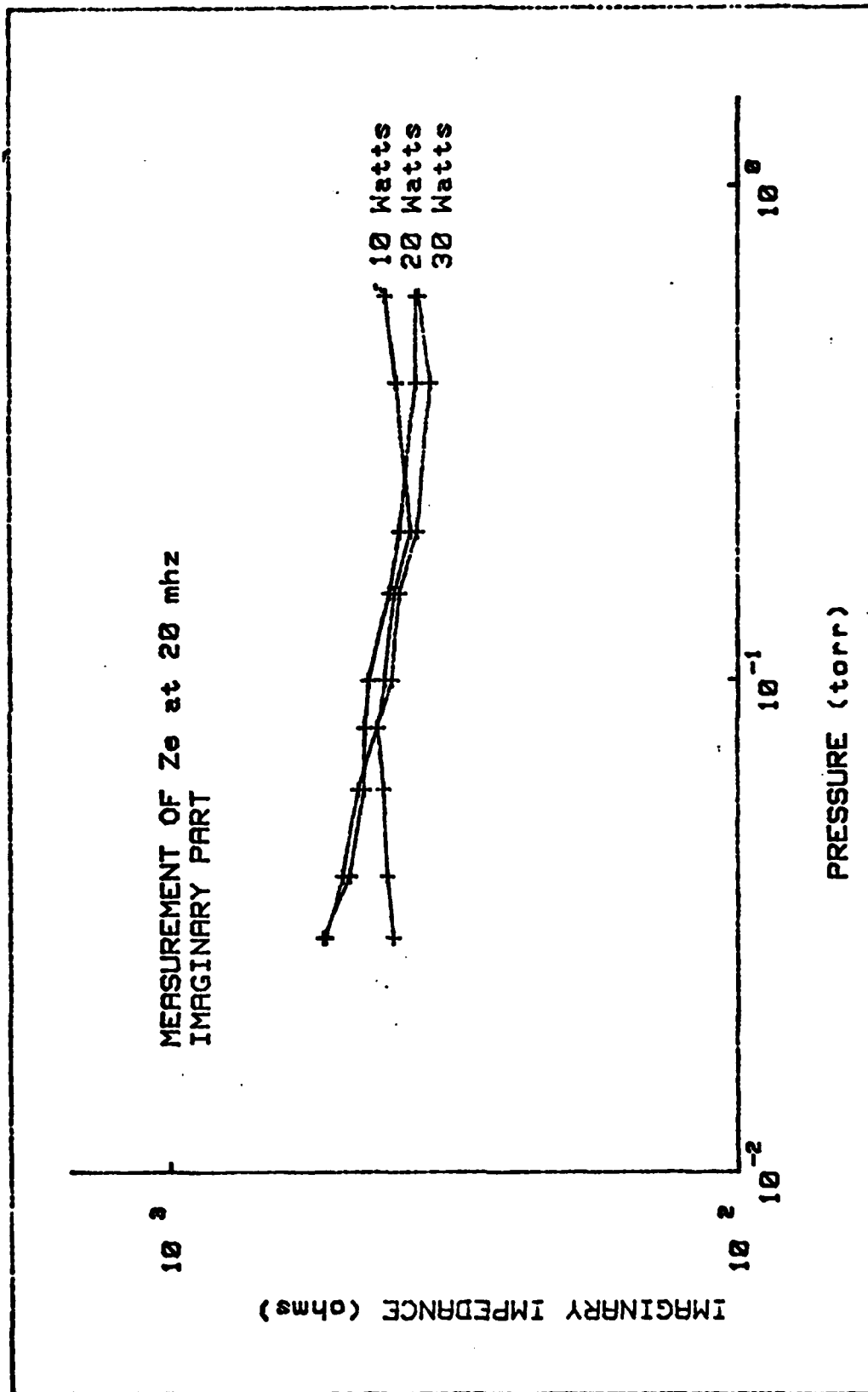


Figure 12. Imaginary Impedance Component

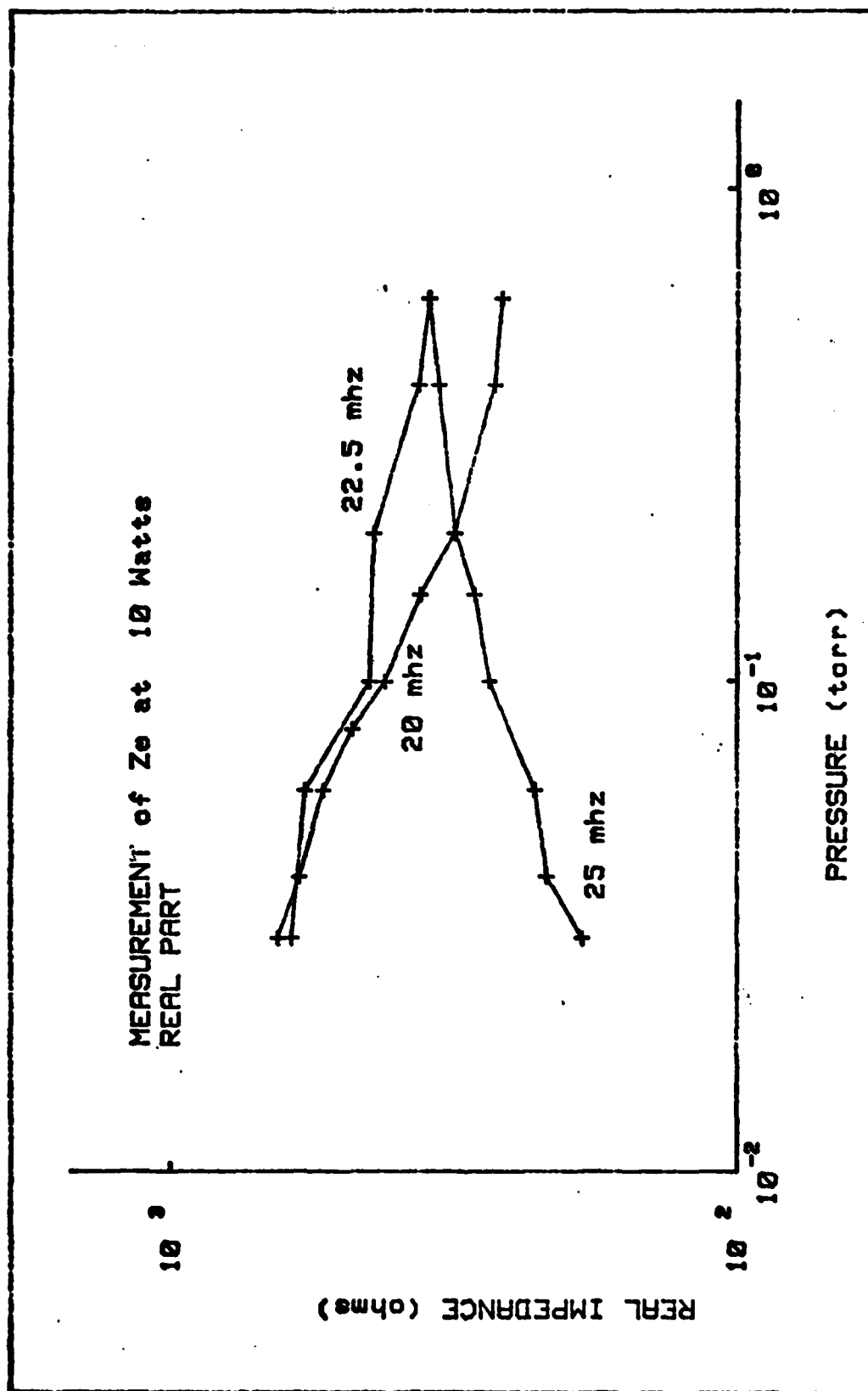


Figure 13. Real Impedance Component

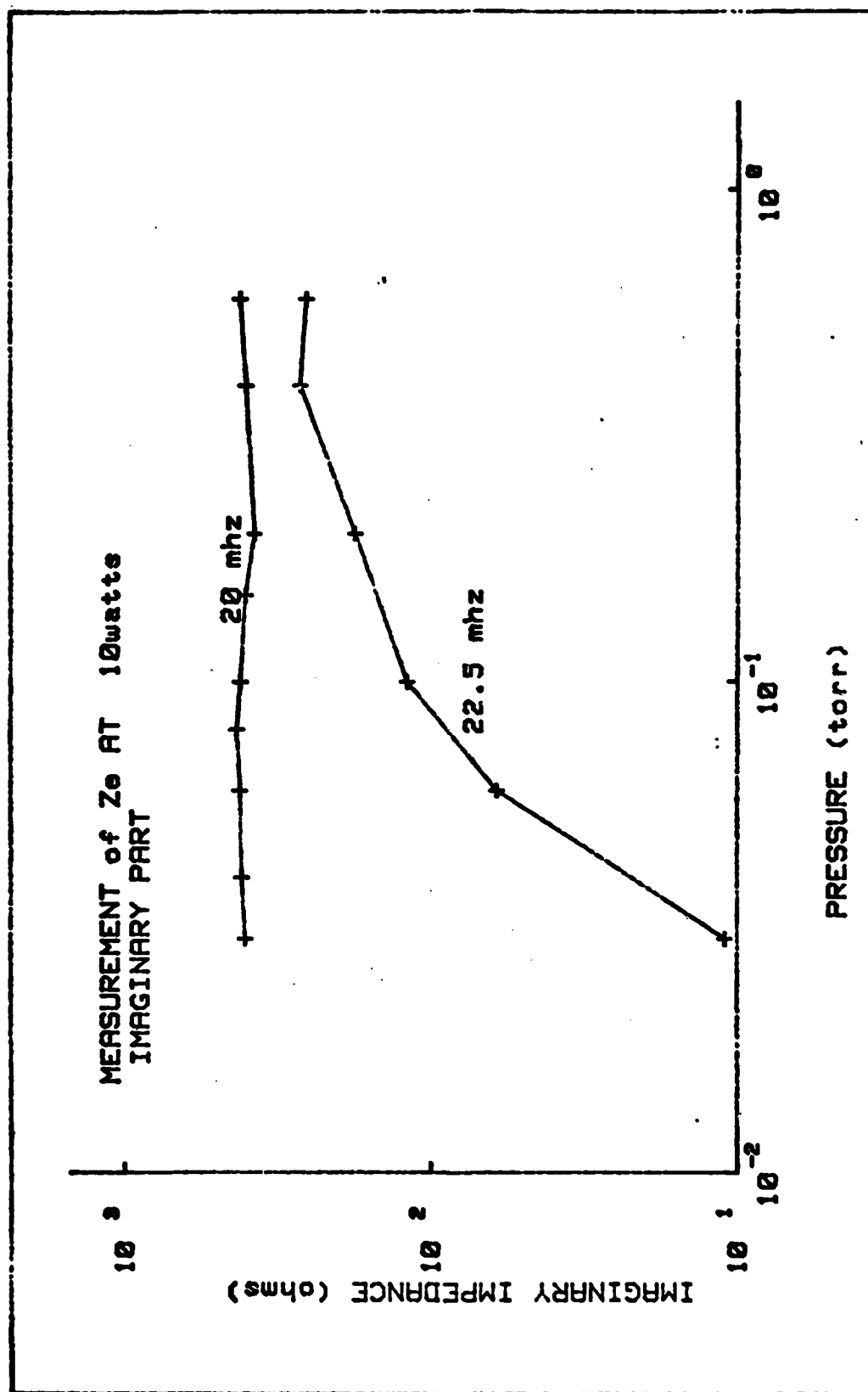


Figure 14. Imaginary Impedance Component

Examples of the data show that the impedance measurably responds to changes in system parameters (power, frequency, pressure, etc.). Figures 11 and 12 show the impedance measured at 20 MHz. The real portion exhibits a common value at low pressure, and has little dependence on pressure until reaching a breakpoint after which it scales inversely with pressure to the 1/3 power. The imaginary portion shows no dependence on pressure within measurement accuracy limits. Figures 13 and 14 show impedance measured at constant power. Changes in frequency produce changes in both the magnitude and slope of the impedance vs pressure curves.

Figures 15 and 16 show plots of the admittance (the reciprocal of impedance) as a function of frequency. Plotted for comparison is the case of an ideal resistor-inductor-capacitor (RLC) circuit using constant component values comparable to those measured. The presence of the plasma has a pronounced effect, increasing with frequency. Figure 16 shows the imaginary portion. Here the ideal circuit would reach a resonance condition near 30 MHz. The plasma results in a resonance near 22 MHz. Treating the plasma as a lossy dielectric should produce the opposite effect. Since the resonant frequency is given by $\omega^2 = (LC)^{-1}$, a reduction in the capacitance would result in a higher resonant frequency. The resistance term (Figure 15) arises in the model from the product of the imaginary term of the permittivity with the imaginary capacitive reactance. Measurements show a deviation

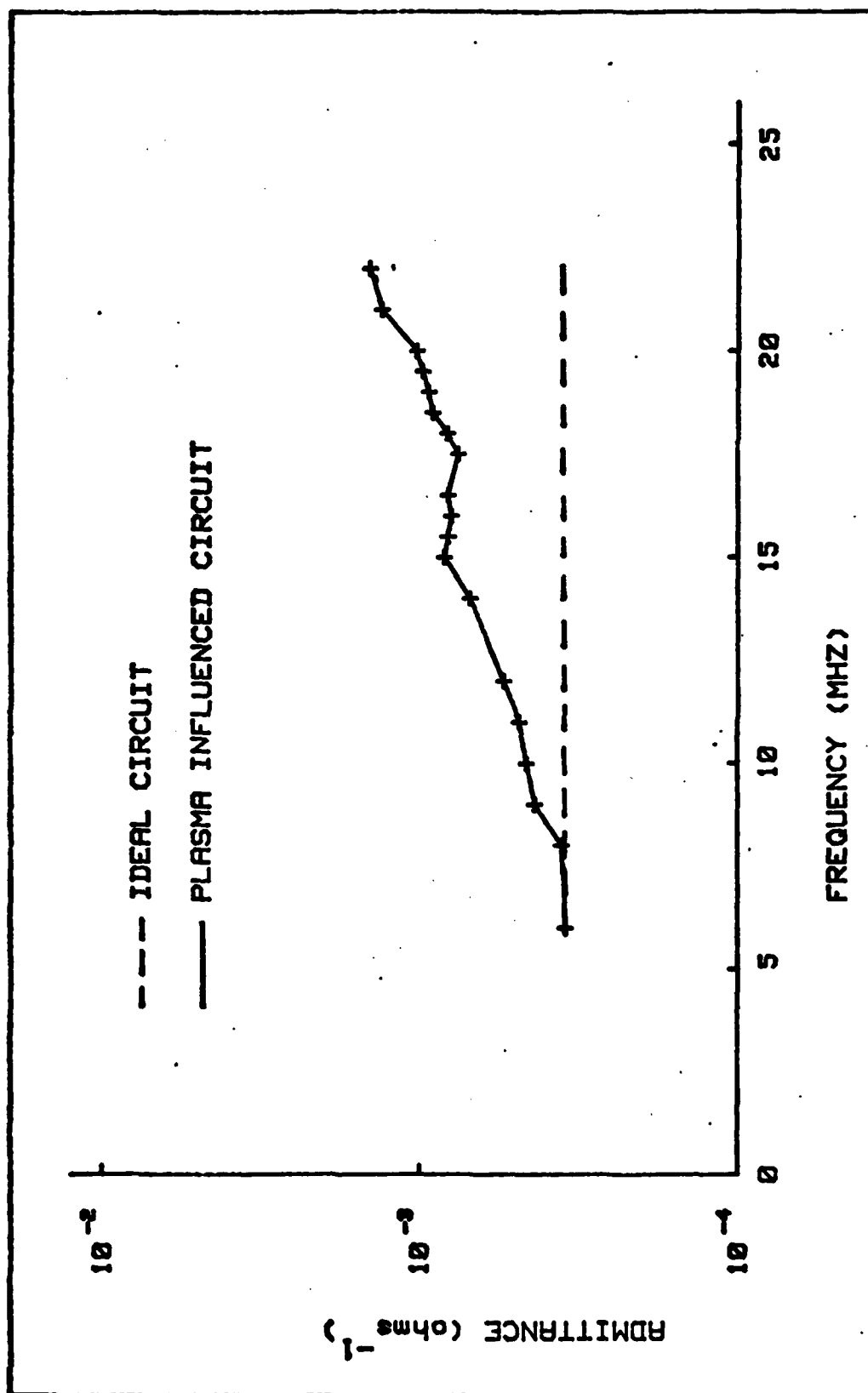


Figure 15. Real Admittance Component

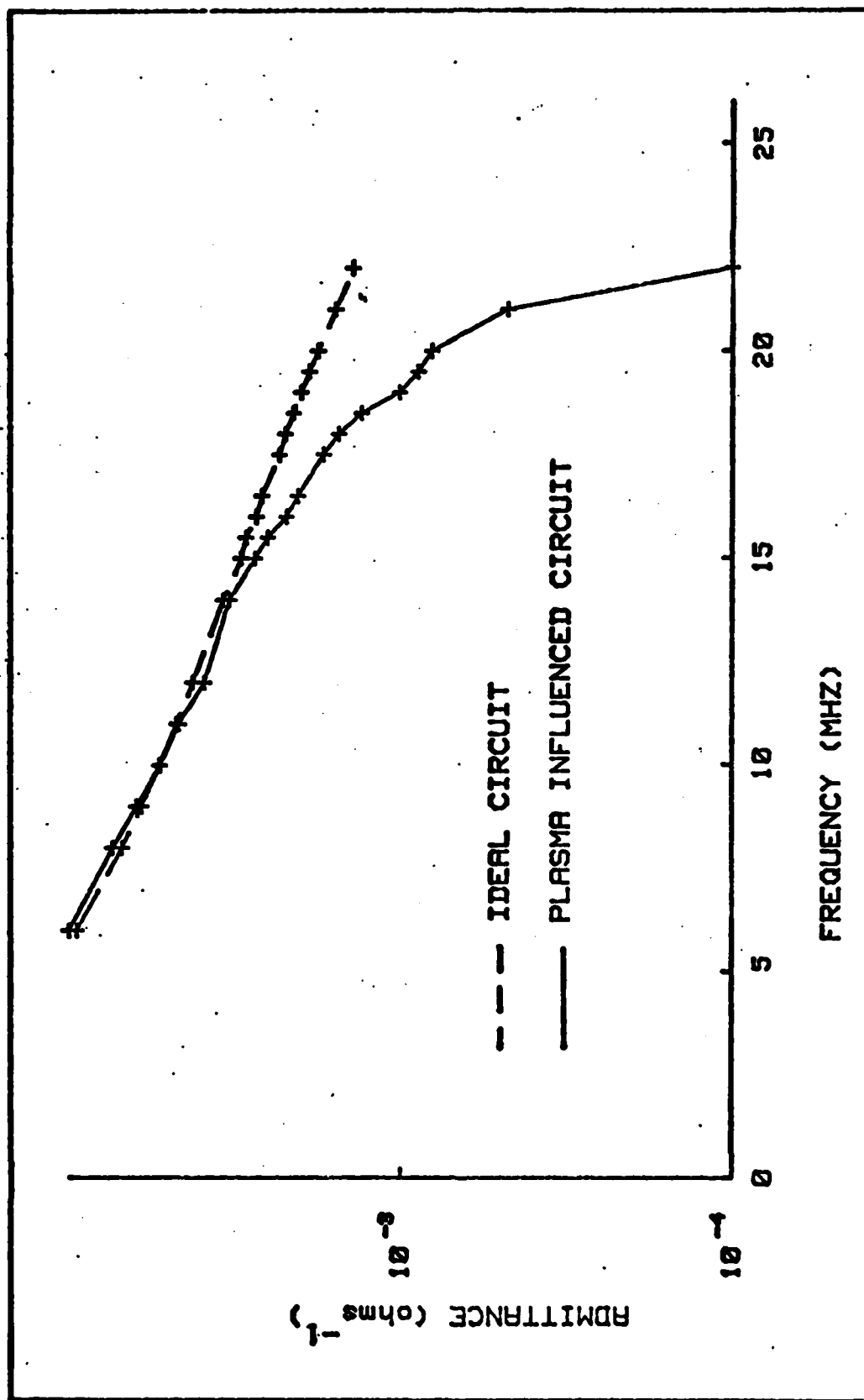


Figure 16. Imaginary Admittance Component

from the ideal circuit. Together these results suggest the plasma-circuit model to be incomplete.

Figures 17 through 20 show reduced data. Under certain sets of conditions, the results agree closely with theory. For example, the slope of the collision frequency vs. pressure curve (Figure 17) is expected by Equation (4) to be 2.4×10^9 . At 20 MHz, this value is correctly calculated at 0.1 torr. The slope of the curve is slightly below expected (1.2×10^9) at lower pressures and slightly higher (4.1×10^9) at higher pressures but the average slope agrees with theory over the entire pressure range investigated. Similar results appear for 22 MHz and 25 MHz. Other selected frequencies, for example, 18 MHz and 28 MHz exhibit a much smaller slope, significantly deviating from theory. Calculated electron number densities exhibited similar trends. However, expected uniform increases with respect to increasing power levels were not observed. Nevertheless, an increase in plasma intensity is visably apparent. To quantify this observation, several Helium emission lines were spectroscopically scanned. A plot of photoconductor current vs. RF input power is shown in Figure 21. Each line examined exhibited a continuous increase over the range of input power.

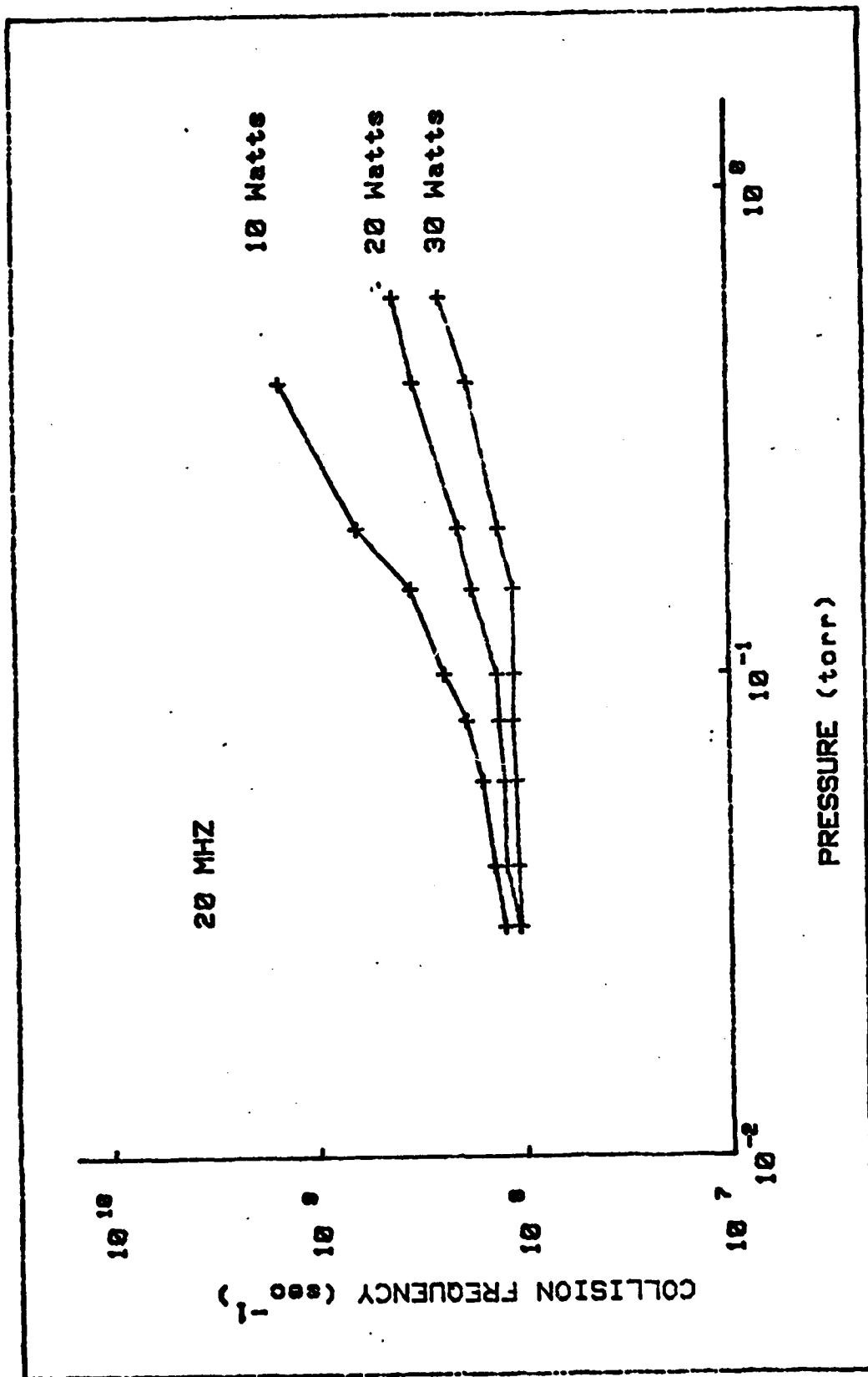


Figure 17. Collision Frequency

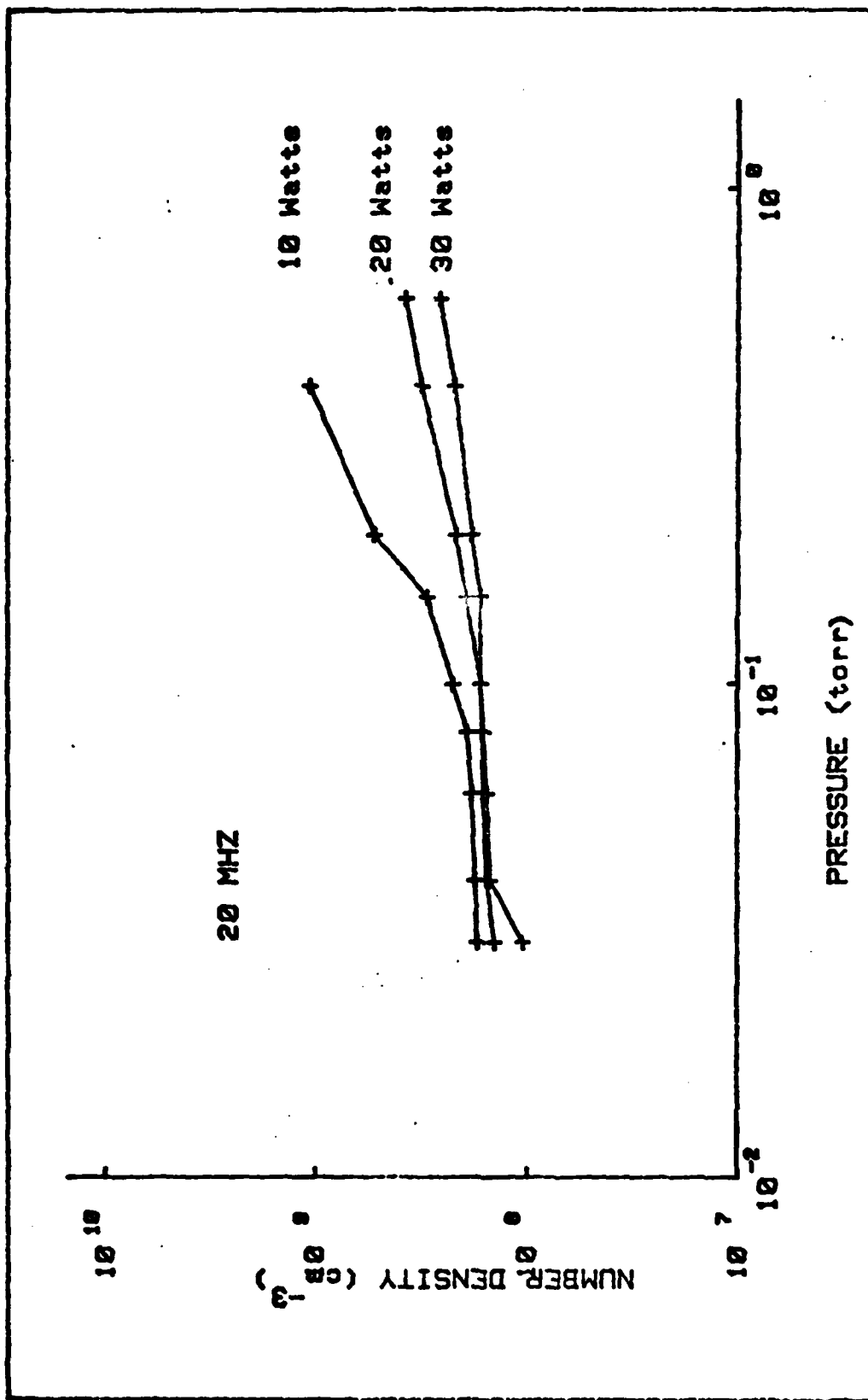


Figure 18. Number Density

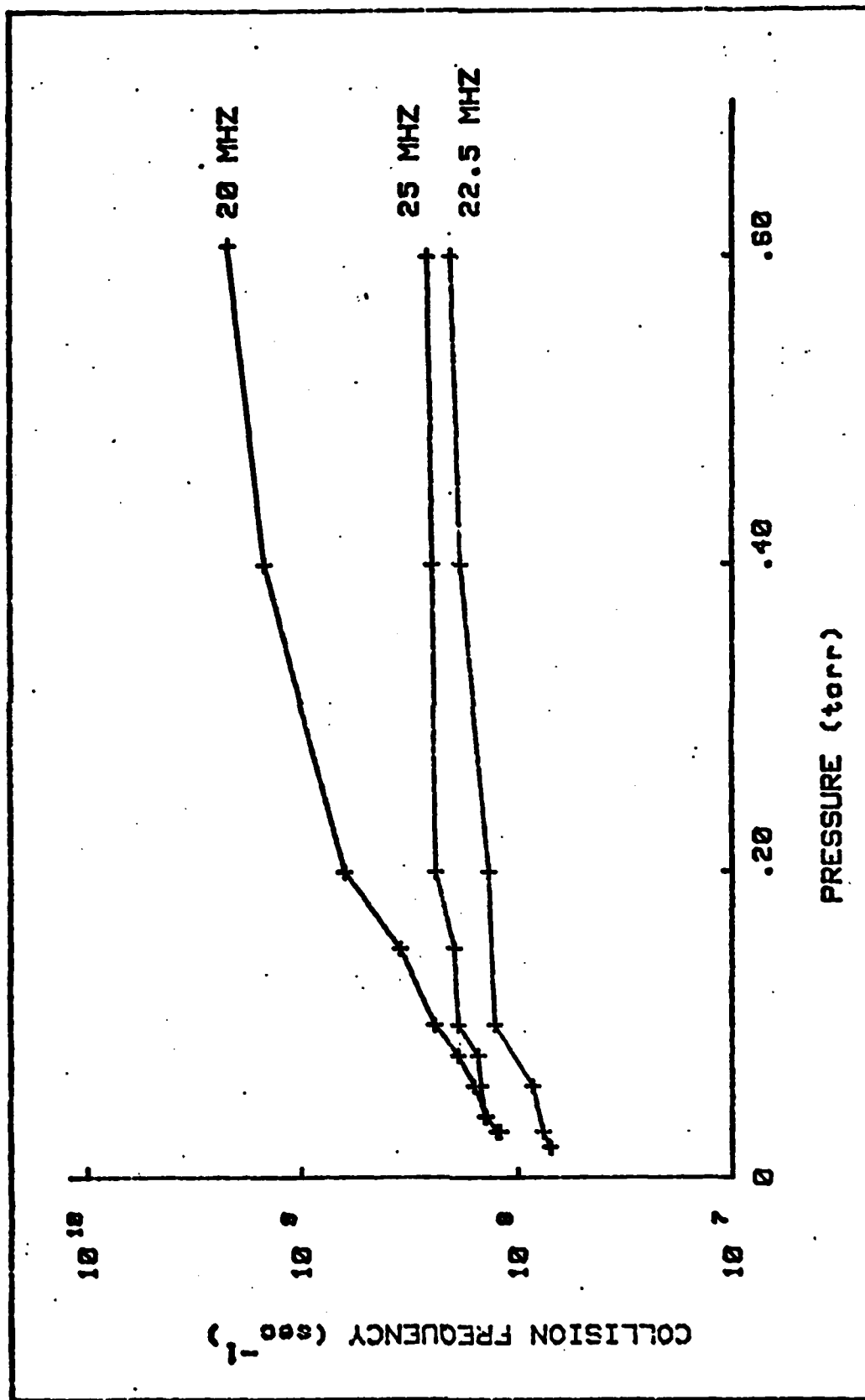


Figure 19. Collision Frequency

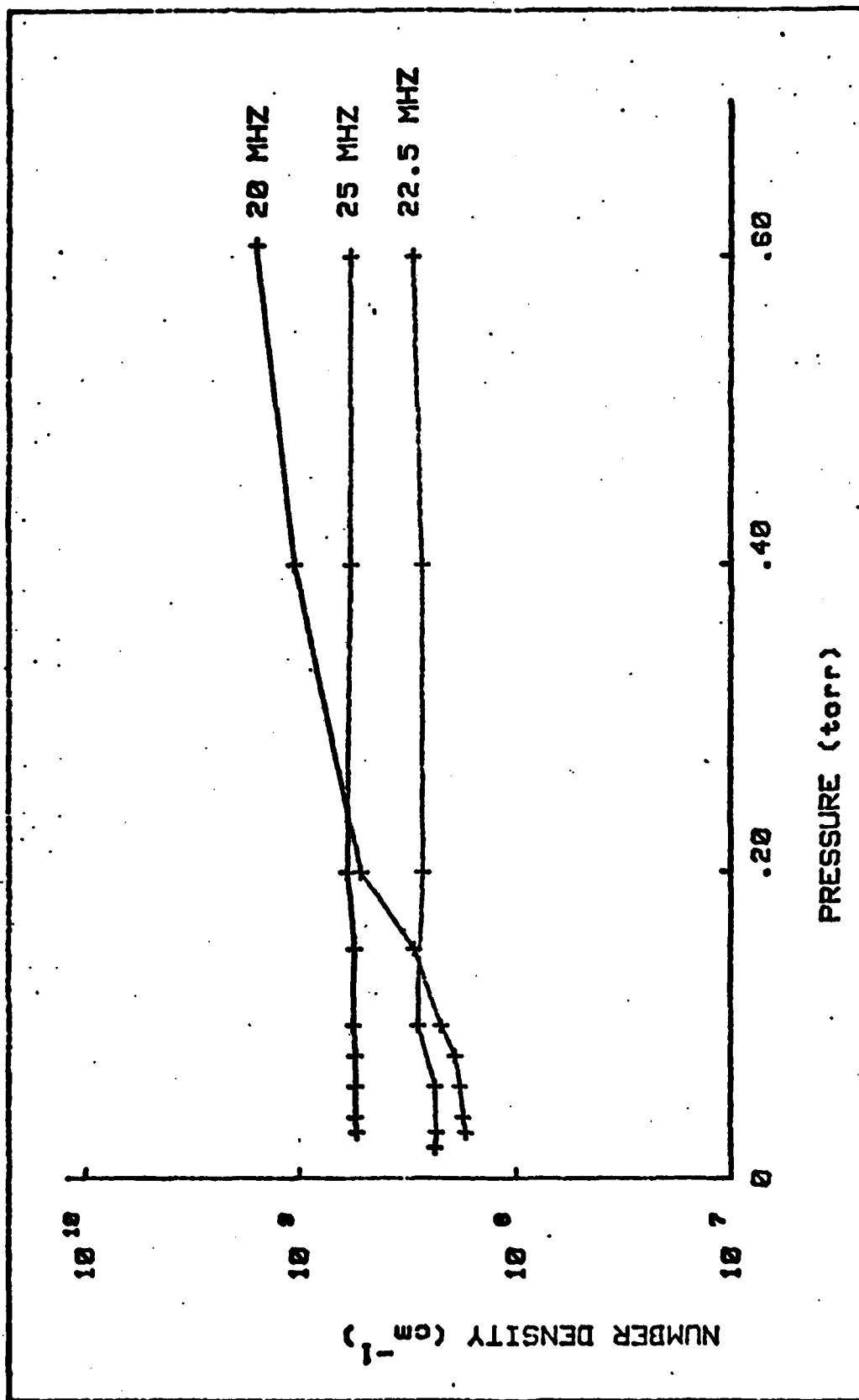


Figure 20. Number Density

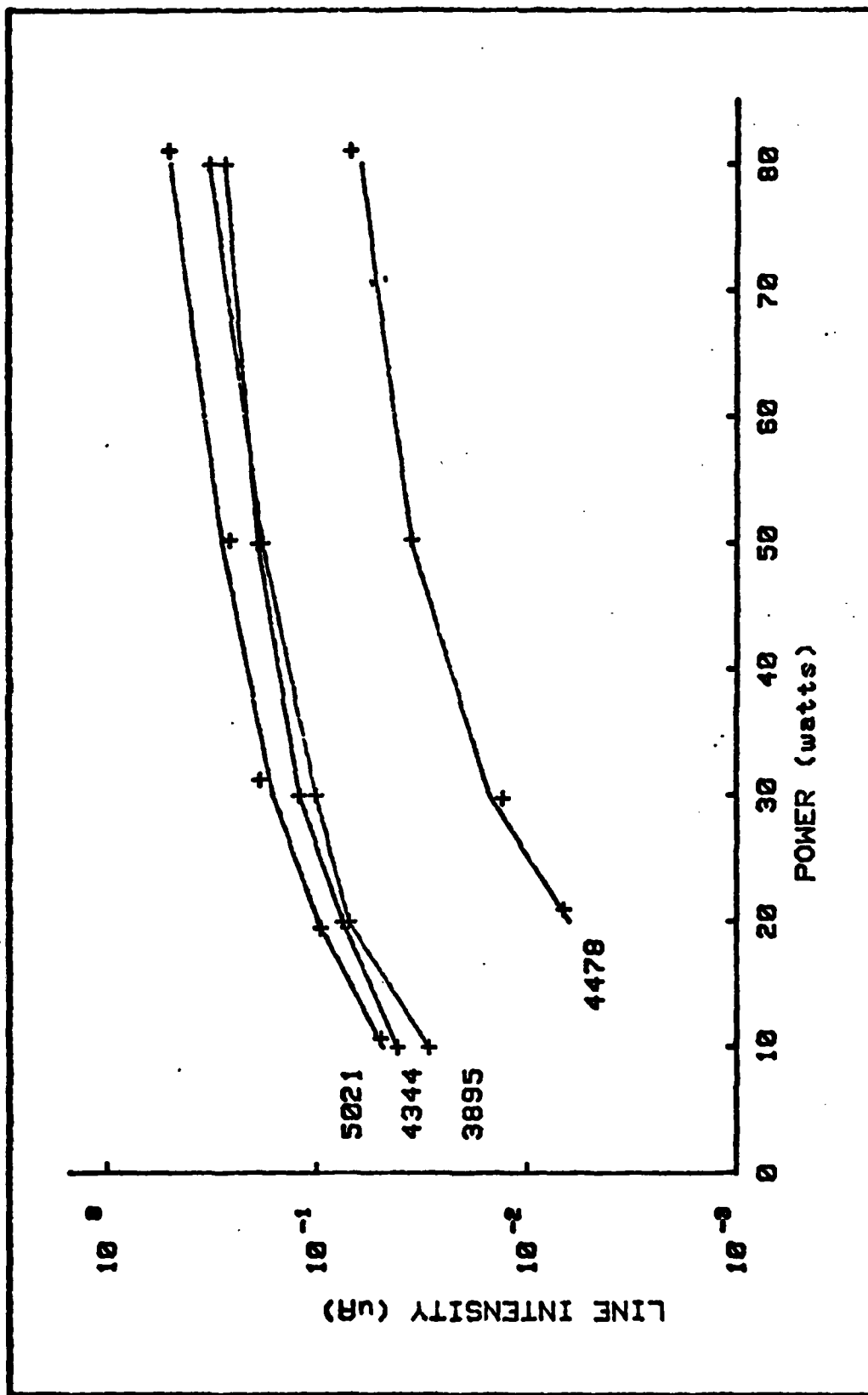


Figure 21. Line Intensities

VI. Conclusion

Summary and Conclusions

The results of this study show that in an inductively driven plasma, there is an observable phenomena which interacts with the driving inductor to produce changes in the electrical circuit impedance. The procedures outlined in Section IV can be used to identify the circuit impedance which exhibits measurable sensitivity with respect to changes in gas pressure, input power or driving frequency. Provided an acceptable circuit model of the plasma is introduced, the measured impedance can be used as a diagnostic to determine the plasma parameters.

In pursuit of this goal, an in depth theoretical and experimental analysis was made of a specific plasma impedance measurement technique applied to an inductively excited RF plasma. Special attention was given to calculation of v and n . Steady state plasma theory was applied to explain predominate electron source and loss mechanisms and basic plasma phenomena.

To relate the plasma to the electrical driving circuit, a plasma-circuit was formulated. Depending heavily on traditional electric circuit analysis but recognizing the nuances of RF energy, a thorough analysis was then performed on the total circuit as well as individual components. Three results evolved. First, the method of data reduction out-

lined by Illic (Illic, D.B., 1981:1544) could not be applied to the existing equipment. Recognition of measurement sensitivity and error propagation indicated that inordinate amounts of RF shielding would be necessary to carry out required matching network calibration. Second, the impedance measurement procedure described in Section IV was conceived. This procedure offers certain advantages over that presented by Illic. Third, equations were developed to calculate plasma parameters from circuit impedance values. For comparison, the suggested development adapted in Appendix B was applied and, although some comparable data was obtained, observable discrepancies could not be solely attributed to either development because of inherent component calibration errors.

More than just a numerical comparison of these two methods is warranted here. A subtle difference exists which accents each's attributes and highlights potential applications. The technique described in Section IV utilizes a direct impedance measurement employing the RF meter described in Section III. The technique presented by Illic and adapted to this study in Appendix B requires precalibration of matching network components in order that control knob settings may be used to provide data input. Both techniques presuppose the impedance matched condition for validity.

It is possible to use these techniques concurrently (although not simultaneously) so as to make two measurements for each matched impedance condition. Illic's method is per-

formed on an operating plasma and has two notable advantages. It provides a real-time measurement and this information can be used as an error signal for plasma control applications. The method conceived in this study requires a power interruption but offers the advantage of using a direct circuit impedance measurement extracted from the driving inductor input close to the plasma, thus eliminating upstream equipment calibrations. Also, being a post plasma measurement, common stray RF propagation effects are eliminated.

Although both methods were applied to the configuration under study, Ilic's equipment incorporated a continuous tuning feature which would destabilize during power interruptions and void post plasma measurements.

The central value of impedance methods is that they are external to the plasma chamber and nondisturbing to either dynamic particle flows or temporal and spatial fields. This is in contrast to techniques such as probes or microwave diagnostics for which substantial study has been done to account for these effects. Also the impedance matched criteria imposed assures maximum power transfer and efficiency which are of significant benefit to industrial users. The contrasting features of the two methods offer alternatives to readers concerned with specific plasma applications.

The plasma-circuit model investigated did not completely account for all phenomena occurring and does not permit accurate calculation of plasma electron number density or electron

neutral collision frequency. Associated changes in stray capacitance and sheaths impose larger effects upon the circuit than do the small changes in plasma parameters of interest.

The portion of the model presenting the most difficulty for analysis is the basic capacitance, C_0 . The magnitude of this term is small (0.5 pf in this experiment) and difficult to obtain. Furthermore, changes to the plasma result in only a percentage change in C_0 (say 10%). The term C_0 , in turn, is only a small portion (5%) of the total parasitic capacitance of the driving inductor and it is this total capacitance that interacts with the electrical circuit. This interaction itself may be only small perturbation at frequencies other than near resonance. The result is that the overall perturbation of the circuit impedance is much less pronounced than the real changes occurring within the plasma. This measurement process is analogous to determining the speed of a car by measuring the Lorentz contraction of its length.

Recognizing the concomitant demand placed on measurement and calculation accuracy, a detailed error analysis was performed on the primary equations used to calculate plasma parameters. The equations show a sensitivity to errors found in the value for circuit reactance. Small measurement errors propagate with little influence to the value of collision frequency and a 10% confidence level may

be assigned. Calculated number density on the other hand is strongly influenced by errors in either the driving inductance or measured reactance. The value for driving inductance can be determined with high accuracy through successive measurements, however, each value of reactance depends upon an individual circuit impedance value. This sensitivity allows for a confidence level of only 25% for electron number density.

In addition to the unresponsive measurement problem just mentioned, there exists a possible model defect which serves to further distort results. The total model capacitance was considered to consist of two terms: C_o , the capacitance interior to the tube, and C_B , the remaining parasitic capacitance of the system. Both terms are determined by the basic geometry of the system and are therefore invariant except for the changes in C_o already attributed to the permittivity function. If the plasma forms a conducting sheath along the container wall, this may introduce an additional capacitive term between the inductor and the plasma. This effect was noted by Robert Olsen while studying the effect on the impedance of a solenoid due to the presence of a center conductor. (Olsen, R.A., 1961:3). The existence of such a term, conductivity dependant, would vary with the plasma number density. Since it is not determined solely by geometry, its magnitude cannot be measured by the same technique used to determine the terms C_o and C_B .

Recommendations

The procedures, models, and results developed and discussed in this study coupled with the preponderance of interest shown by the plasma physics community warrants further research into the study, and application of plasma impedance diagnostics. Research should include both capacitive and inductive reactors. Measurement sensitivity and the disturbing effect of stray electrical coupling dictate that inductively oriented research be slanted toward specific applications where parameters such as frequency or power can be constrained within narrow limits.

In addition, the simple plasma-circuit model tested in this study was found to be incomplete. A model which would better account for observed effects is shown in Figure 22. This model is equivalent to the model tested over a limited frequency range (Hayt, W.H., 1962:458). Also, the resistor in series with the inductor would account for real resistance in the system while the resistor in parallel with the capacitor would absorb the plasma induced resistive term.

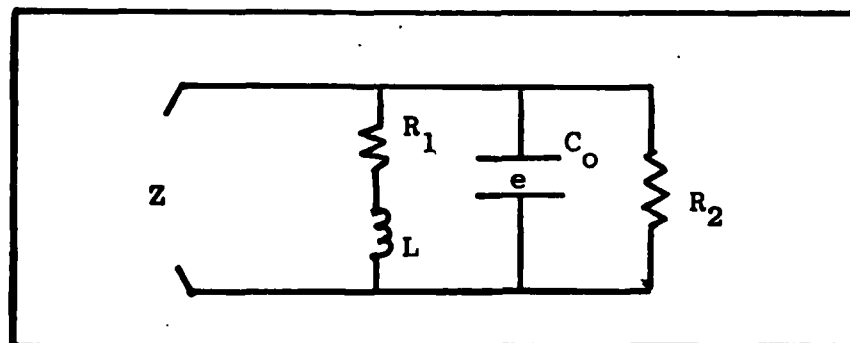


Figure 22. Modified Model

The substitution of a capacitive type plasma reactor into the present system greatly simplifies the model needed and offers good promise of producing significant results. It is likely that once configured, numerical relations could be quickly verified using a Helium plasma before continuing with a spectroscopic study of a molecular gas. The design offered in Figure 23 is currently being fabricated by the sponsor of this thesis. It is a high vacuum, parallel plate reactor incorporating a micrometer controlled, 5 cm travel plasma cavity. Opposing optical windows are included to facilitate spectroscopic analysis.

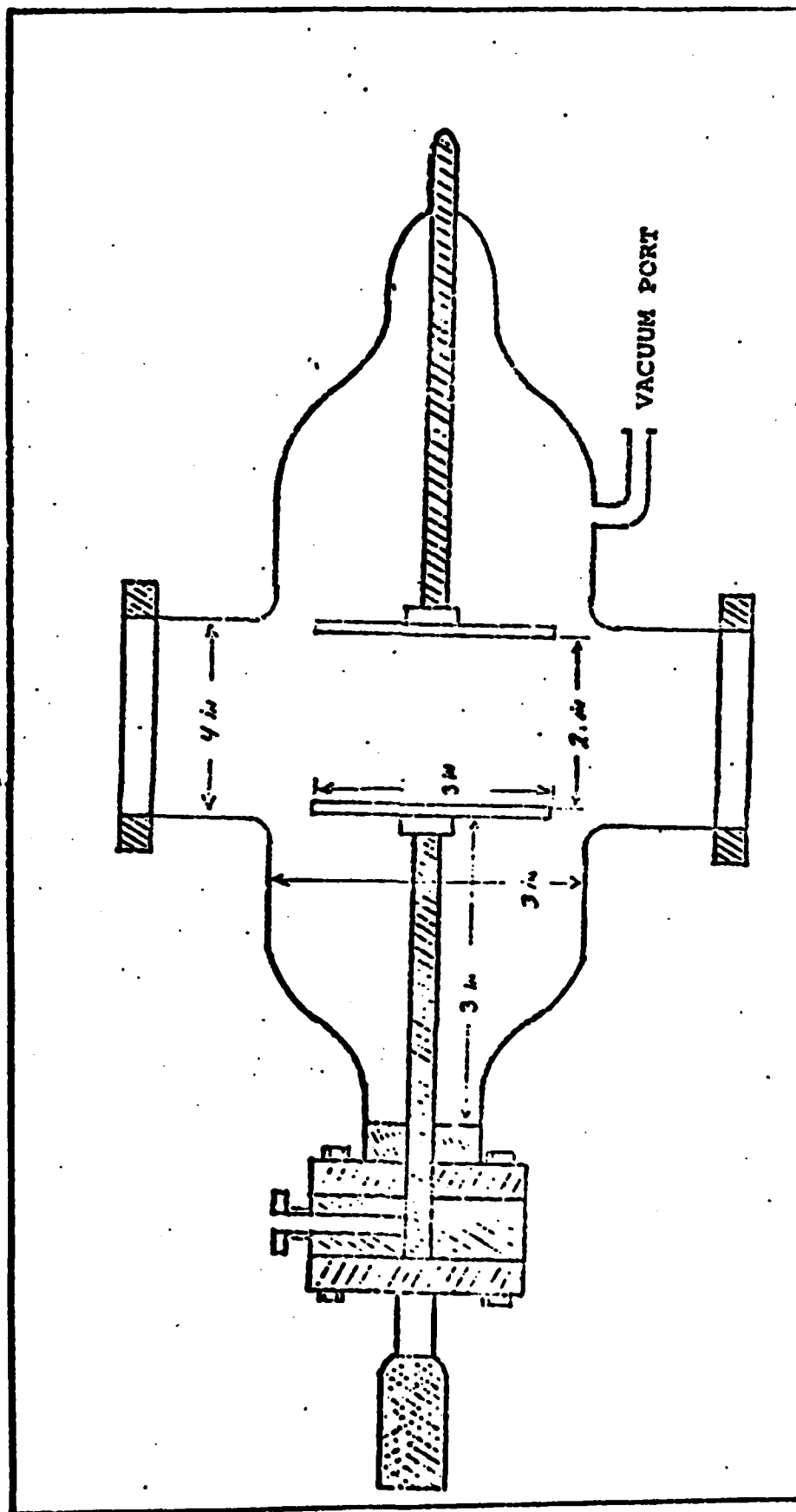


Figure 23. Compactive Reactor Design

Bibliography

1. Brown, S. C. Introduction to Electrical Discharges in Gases. New York: John Wiley and Sons, 1966.
2. Brown, S. C. Basic Data of Plasma Physics. Cambridge, Mass.: The M.I.T. Press, 1967.
3. Chen, F. F. Introduction to Plasma Physics. New York: Plenum Press, 1977.
4. Hayt, W. H. Engineering Circuit Analysis. New York: McGraw-Hill, 1962.
5. Hirsh, M. N. and Oskam, H. J. Gaseous Electronics. New York: Academic Press, 1978.
6. Illic, D. B. "Impedance Measurement as a Diagnostic for Plasma Reactors", Review of Scientific Instruments, 52: 1542-1545 (October 1981).
7. Illic, D. B. "Thin Film Formed by Plasma Enhanced Chemical Vapor Deposition", Hewlett Packard Journal, 33: 20-27 (August 1982).
8. Marion, J. B. and Head, M. A. Classical Electromagnetic Radiation. New York: Academic Press, 1980.
9. Marr, G. V. Plasma Spectroscopy. London: Elsevier Publishing, 1968.
10. Norstrom, H. "Experimental and Design Information for Calculating Impedance Matching Networks for Use in RF Sputtering and Plasma Chemistry", Vacuum, 29: 341-350 (October 1979).
11. Olsen, R. A. "Measurement of Plasma Conductivity Employing an Electrodeless Technique", Report M-1282-1, United Aircraft Corporation Research Laboratories, 1961.
12. Sanders, S. G. "Plasma Rate Equations for an RF Discharge in a Magnetic Field", Journal of Applied Physics, 49: 2689-2695 (May 1978).
13. Stamm, M. R., Associate Professor of Physics. Class Notes, PH 6.20, Air Force Institute of Technology, Wright-Patterson Air Force Base, Ohio, 1982.
14. Tang, J. T., et al. "Temporal and Spatial Measurement of RF Electric Field in a Magnetized Plasma Using an Emissive Probe", Review of Scientific Instruments, 50: 1458-1460 (November 1979).

Appendix A
Data Reduction

The equations developed here represent an independent analysis of the electrical circuit and the relationship between measurements and plasma parameters. The circuits shown in Figure 4 are applicable here. We recall:

$$Z_p = \frac{1}{i\omega(C_B + e_p C_o)} \quad (38)$$

We chose to write the permittivity expression in the following form:

$$e_p = 1 - \frac{\omega_p^2}{\omega^2 + \nu^2} - i \frac{\omega_p^2 \nu}{\omega(\omega^2 + \nu^2)} \quad (39)$$

Combining the parallel circuit elements and making the appropriate substitutions gives the expressions:

$$\frac{1}{Z_e} = \frac{1}{Z_L} + \frac{1}{Z_p} \quad (40)$$

$$\frac{1}{Z_e} = \frac{\nu n_e C_o}{\omega^2 + \nu^2} + i\omega \left[C_B + C_o - \frac{n_e C_o}{\omega^2 + \nu^2} - \frac{1}{\omega^2 L} \right] \quad (41)$$

The term $\frac{1}{Z_e}$ can be set equal to some real and imaginary parts, R'_e and X'_e , where the primes indicate that the values relate to a reciprocal impedance. Separating the parts, solving

simultaneously and inserting the previously defined term γ produces the following set of equations:

$$\gamma = \frac{-\omega R'_e}{X'_e - \omega C_o - \frac{1}{\omega^2 L}} \quad (42)$$

$$n_e = \frac{R'_e(\omega^2 + \gamma^2)}{\gamma C_o} \quad (43)$$

values for R'_e and X'_e are readily determined from a measurement of Z_e and the use of a calculator program labeled "NUE" which can be found in Appendix C.

Appendix B
Data Reduction

The original concept of this study was to develop a method of determining plasma parameters from the matching network dial settings. This was accomplished by calibrating the frequency dependant impedance of the tuner and transmission cable and borrowing equations developed in previous portions of this study. When all impedances are matched, the signal generator drives a purely resistive load of $Z_o = 50$ ohms. Labeling the tuner impedance as Z_t and the transmission line impedance as Z_m , we can write the equivalent impedance as:

$$Z_e = Z_o - Z_t - Z_m \quad (44)$$

Separating into real and imaginary parts gives the following:

$$R_e = 50 - (R_t + R_m) \quad (45)$$

$$X_e = - (X_t + X_m) \quad (46)$$

Once the desired frequency is selected, a measurement of the transmission line gives a value for the associated impedance. Extensive use of this method would suggest calibrating the transmission line over a continuous range of frequency thereby avoiding replicating this measurement. The matching net-

work dial settings are read at the impedance matched point. These dial settings correspond to values of the tuner components, C_1 , C_2 , and L obtained from calibration curves shown in Figures 24, 25, and 26. These values can be reduced by circuit analysis (a short computer program was written to perform repeated calculations) to yield a value for the combined tuner impedance. Equations (45) and (46) then give values which reduce to a single impedance given by the equation:

$$Z_p = \frac{-\omega L X_e - i\omega L R_e}{-R_e + i(\omega L - X_e)} \quad (47)$$

The real and imaginary parts of Z_p are then used in the calculator program labeled "ZIP" (See Appendix C) to calculate values for collision frequency and number density.

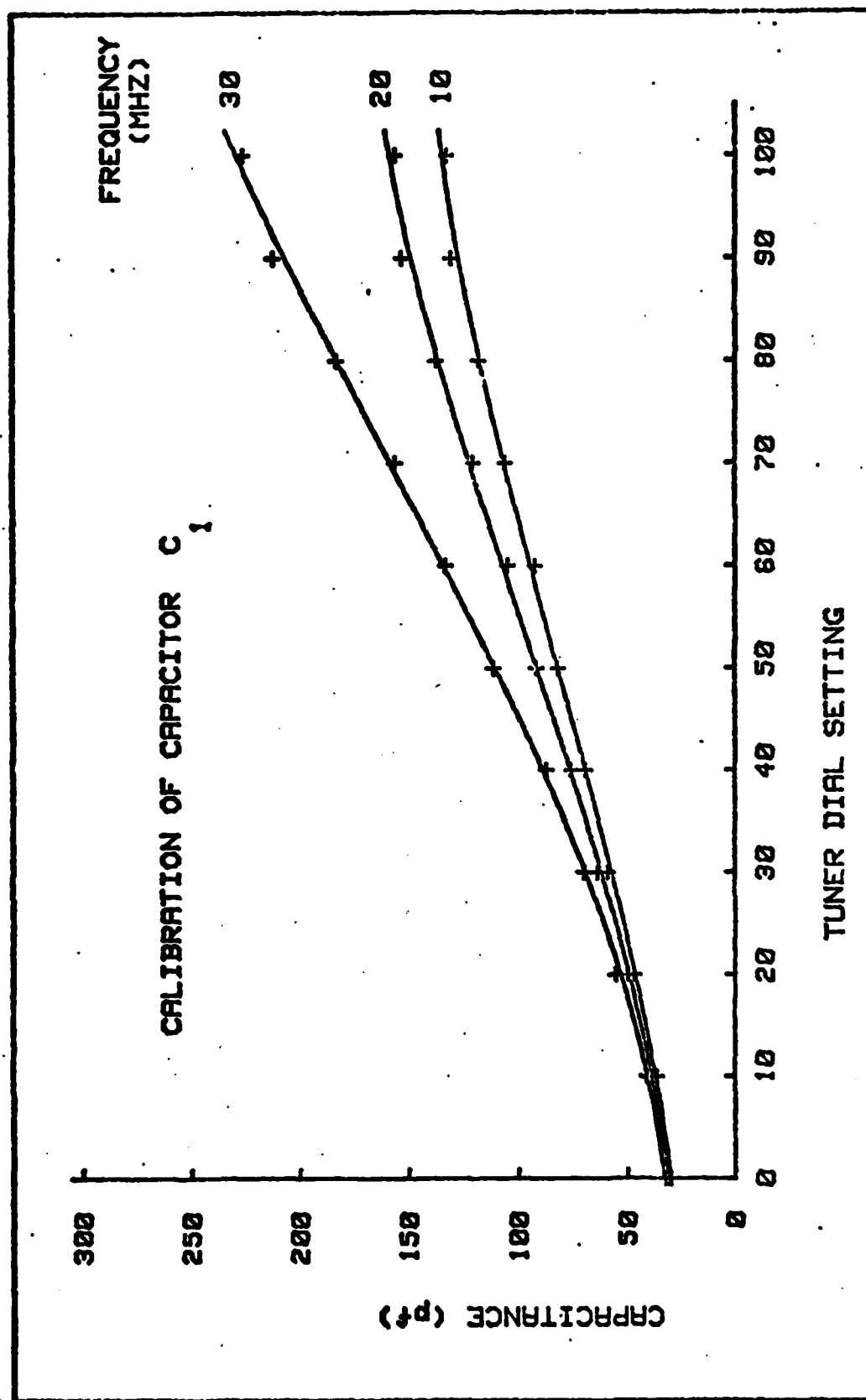


Figure 24. Capacitor Calibration

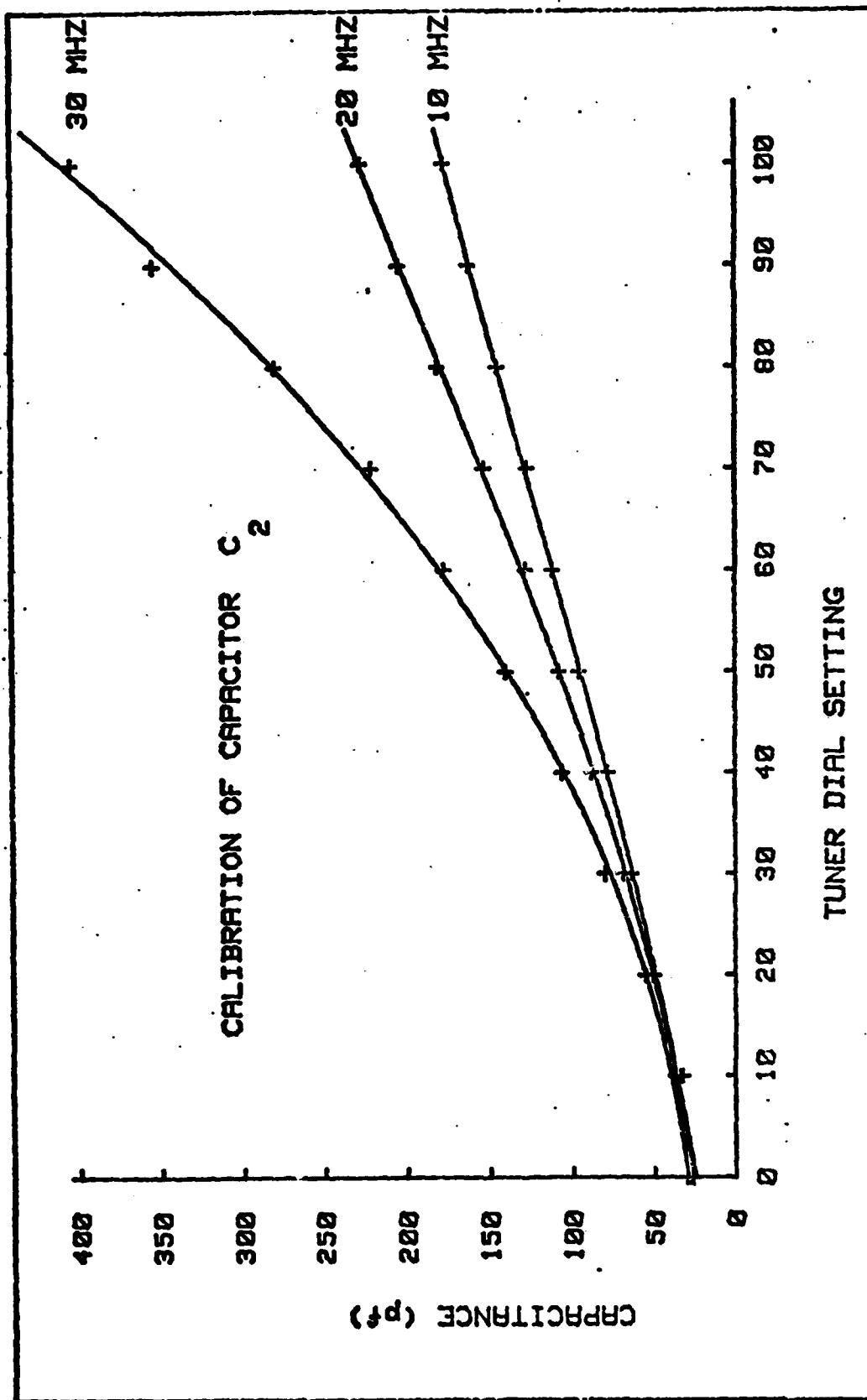


Figure 25. Capacitor Calibration

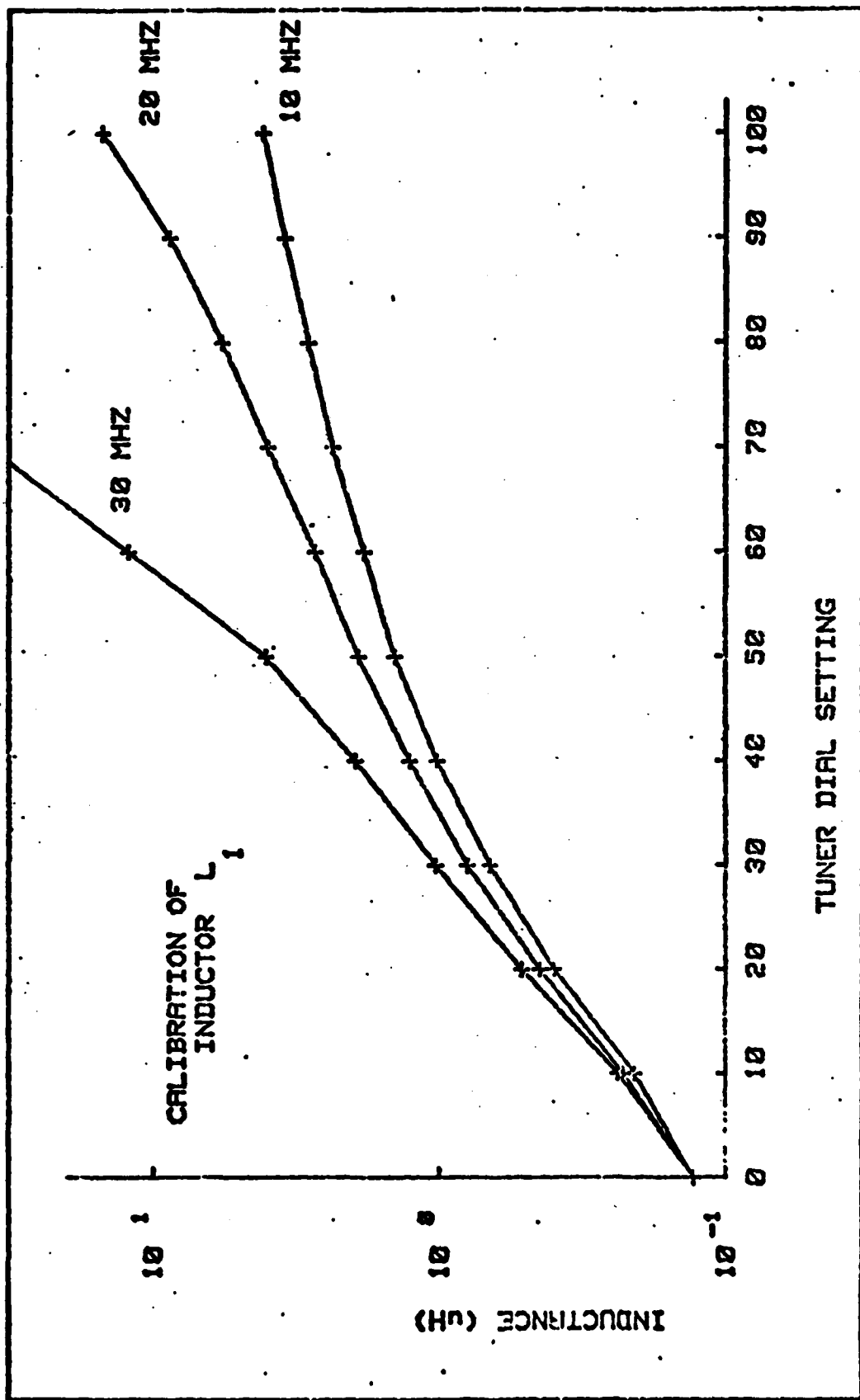


Figure 26. Inductor Calibration

Appendix C
Computer Programs

The following two program are designed for use on the Hewlett-Packard Model HP-41C programmable calculator.

Program "NUE" or "ZIP"

Initialize program

Store w in register 06.

Store the phase of Z_{cable} in register Y.

Store the magnitude of Z_{cable} in register X.

Program:

```
01. LBL NUE
02. X--Y
03. CHS
04. X--Y
05. P-R
06. XROM CINV
07. STO 11
08. RDN
09. STO 12
10. RCL 06
11. X2
12. STO 13
13. 2.70 E-6
14. *
15. 1/x
16. CHS
17. 8.92 E-12
18. +
```

19. RCL 06
20. *
21. CHS
22. RCL 12
23. +
24. 1/x
25. RCL 11
26. *
27. RCL 06
28. *
29. STO 02
30. NUE
31. ARCL X
32. AVIEW
33. RCL 02
34. X^2
35. RCL 13
36. +
37. RCL 11
38. *
39. STO 14
40. 3.182 E9
41. RCL 02
42. *
43. 0.52 E-12
44. *
45. RCL 14
46. X--Y
47. /
48. STO 03
49. Ne =
50. ARCL X
51. AVIEW
52. END

Program:

01. LBL ZIP
02. X--Y
03. CHS
04. X--Y
05. P-R
06. STO 11
07. RDN
08. STO 12
09. Store R_X
10. PROMPT
11. RCL 06
12. 2.70 E-6
13. *
14. STO 13
15. RCL 12
16. -
17. STO 14
18. RCL 12
19. RCL 13
20. *
21. CHS
22. STO 15
23. RCL 11
24. RCL 13
25. *
26. RCL 15
27. RCL 14
28. RCL 11
29. CHS
30. XROM C/
31. STO 11
32. RDN
33. STO 12

34. 17.2
35. STO 13
36. 0.52 E-12
37. STO 14
38. RCL 06
39. *
40. STO 17
41. 1/x
42. RCL 12
43. *
44. STO 15
45. RCL 12
46. X^2
47. RCL 13
48. *
49. STO 16
50. RCL 11
51. X^2
52. RCL 13
53. *
54. RCL 16
55. +
56. RCL 15
57. +
58. STO 15
59. RCL 14
60. *
61. 1/x
62. RCL 11
63. *
64. STO 07
65. NUE =
66. ARCL X
67. AVIEW
68. RCL 12

69. RCL 13
70. *
71. RCL 17
72. 1/x
73. +
74. STO 18
75. RCL 17
76. RCL 15
77. *
78. 1/x
79. RCL 18
80. *
81. RCL 13
82. +
83. RCL 06
84. X^2
85. *
86. 3.182 E9
87. /
88. Ne =
89. ARCL X
90. AVIEW
91. END

Vita

Captain Thomas W. Hermanson was born in Michigan on April 16, 1949. He attended college at Central Michigan University and Grand Valley State College, receiving a Bachelor of Science Degree in Physics. He received his commission from Officer Training School in November 1971. He completed pilot training at Vance AFB, Oklahoma in January 1973. He was assigned to the 1866 Flight Facilities Checking Squadron, Richard-Gebaur AFB, Missouri, from 1973 to 1975; the 11 Tactical Drone Squadron, Davis Monthan AFB, Arizona, from 1975 to 1978; and the 8 Special Operations Squadron, Hurlburt Field, Florida, from 1978 to 1981. He completed one year of study in the Master of Science Program in Management at Troy State University before being assigned to the School of Engineering, Air Force Institute of Technology, Wright-Patterson AFB, Ohio.

Permanent Address: 3620 Countryplace Lane
Sarasota, Florida 33583

UNCLASSIFIED

SECURITY CLASSIFICATION OF THIS PAGE (When Data Entered)

REPORT DOCUMENTATION PAGE		READ INSTRUCTIONS BEFORE COMPLETING FORM
1. REPORT NUMBER AFIT/GEP/PH/82D-12	2. GOVT ACCESSION NO. AD-A124790	3. RECIPIENT'S CATALOG NUMBER
4. TITLE (and Subtitle) PLASMA ELECTRON NUMBER DENSITY AND ELECTRON NEUTRAL COLLISION FREQUENCY FROM COMPLEX IMPEDANCE MEASUREMENTS		5. TYPE OF REPORT & PERIOD COVERED MS THESIS
7. AUTHOR(s) THOMAS W. HERMANSON CAPTAIN USAF		6. PERFORMING ORG. REPORT NUMBER
9. PERFORMING ORGANIZATION NAME AND ADDRESS AIR FORCE INSTITUTE OF TECHNOLOGY (AFIT/EN) WRIGHT-PATTERSON AFB OHIO 45433		8. CONTRACT OR GRANT NUMBER(s)
11. CONTROLLING OFFICE NAME AND ADDRESS AIR FORCE WRIGHT AERONAUTICAL LABORATORY WRIGHT-PATTERSON AFB OHIO 45433		10. PROGRAM ELEMENT, PROJECT, TASK AREA & WORK UNIT NUMBERS
14. MONITORING AGENCY NAME & ADDRESS (if different from Controlling Office)		12. REPORT DATE DECEMBER 1982
		13. NUMBER OF PAGES 85
		15. SECURITY CLASS. (of this report) UNCLASSIFIED
		15a. DECLASSIFICATION/DOWNGRADING SCHEDULE
16. DISTRIBUTION STATEMENT (of this Report) APPROVED FOR PUBLIC RELEASE; DISTRIBUTION UNLIMITED.		
17. DISTRIBUTION STATEMENT (of the abstract entered in Block 20, if different from Report)		
18. SUPPLEMENTARY NOTES Approved for public release: IAW AFR 190-17. <i>Lynn E. Wolaver</i> LYNN E. WOLAVER Dean for Research and Development Development Air Force Institute of Technology (AFIT) Wright-Patterson AFB OH 45433 6 JAN 1983		
19. KEY WORDS (Continue on reverse side if necessary and identify by block number) Plasma Impedance Inductive Plasma Reactor Plasma Reactors Plasma Diagnostic Inductive Plasma		
20. ABSTRACT (Continue on reverse side if necessary and identify by block number) The plasma within an RF driven inductive coil interacts with the electrical generation circuit providing feedback useful for control of bulk plasma parameters. An investigation, employing a tunable RF circuit, was made applying complex impedance measurements as a plasma diagnostic. Plasma-circuit effects are modeled as capacitive coupling to the driving inductor; the magnitude of the plasma model capacitance being proportional to a complex plasma permittivity. Associated impedance, when annulled by tuning, results in a real resistive load		

INCLASSIFIED

SECURITY CLASSIFICATION OF THIS PAGE(When Data Entered)

dependant upon plasma characteristics. Impedance diagnostics avoids the use of traditional internal probes. Application of this technique to inductive reactors is found to be inferior to capacitive reactors.

SECURITY CLASSIFICATION OF THIS PAGE(When Data Entered)